Article:
Gouiza, M orcid.org/0000-0001-5438-2698, Bertotti, G and Andriessen, PAM (2018) Mesozoic and Cenozoic thermal history of the Western Reguibat Shield West African Craton). Terra Nova, 30 (2). pp. 135-145. ISSN 0954-4879

https://doi.org/10.1111/ter.12318

Mesozoic and Cenozoic thermal history of the western Reguibat Shield (West African Craton)

Mohamed Gouiza (corresponding author)

University of Leeds

School of Earth and Environment

Leeds LS1 9JT, UK

+44 7985 78 20 73

m.gouiza@leeds.ac.uk

ORCID: 0000-0001-5438-2698

Giovanni Bertotti

TU Delft

Faculty of Civil Engineering and Geosciences

Stevinweg 1, 2628 CN Delft, Netherlands

Paul A. M. Andriessen

VU University Amsterdam

Faculty of Earth Sciences

De Boelelaan 1085, 1081 HV Amsterdam, Netherlands

Short title: Thermal history of the Western Reguibat Shield

Abstract

Using low-temperature thermochronology on apatite and zircon crystals, we show that the Western Reguibat Shield, located in the northern part of the West African Craton, experienced major cooling and heating events between Jurassic and present times. The obtained apatite fission track ages range between 49 and 102 Ma with mean track lengths varying between 11.6 and 13.3 µm and Dpar values between 1.69 and 3.08 µm. Zircon fission track analysis yielded two ages of 159 and 118 Ma. Apatite (U-Th)/He uncorrected single-grain ages range between 76 and 95 Ma. Thermal inverse modelling indicates that the Reguibat Shield exhumed during the Early Cretaceous, Late Cretaceous, Palaeocene—Eocene, and Quaternary. These exhumation events were coeval with regional tectonic and geodynamic events, and were probably driven by a combined effect of plate tectonics and mantle dynamics.

Introduction

A substantial number of studies examining the thermal evolution of domains contiguous to the Moroccan Atlantic margin reveal the existence of major thermal events that occurred after the initiation of the Early-Middle Jurassic drifting in the Central Atlantic (e.g. Ghorbal *et al.*, 2008; Ghorbal, 2009; Sebti *et al.*, 2009; Saddiqi *et al.*, 2009; Ruiz *et al.*, 2011; Oukassou *et al.*, 2013; Sehrt, 2014; Leprêtre *et al.*, 2014; 2015). These thermal events, constrained by low-temperature thermochronology (LTT) (i.e. fission track and U-Th/He analyses on apatite and zircon crystals), are systematically attributed to km-scale vertical movements of the continental crust (i.e. burial and exhumation). The supposedly exhumed domains are characterized by exposed old pre-Mesozoic basement, and the absence of sedimentary cover prevents from understanding and quantifying the tectonic processes that might have driven such evolution (Teixell *et al.*, 2009; Gouiza, 2011).

The Reguibat shield is a domain that experienced at least one major cooling event during Mesozoic times (Leprêtre *et al.*, 2014; 2015). It is located in the northern part of the West African Craton and extends over 1400 km from the Algerian Sahara domain in the east to the Moroccan Atlantic margin in the west (Fig. 1). It is an ENE-WSW basement rise where Archean and Palaeoproterozoic rocks are exposed (Fig. 1) (Villeneuve and Cornée, 1994; Schofield *et al.*, 2012). It is surrounded by the Variscan Mauritanides Belt in the SW (ca. 300 Ma; Lécorché *et al.*, 1983; Purdy, 1987), the coastal Atlantic basin of Tarfaya in the NW, the Palaeozoic Tindouf Basin in the N-NE, and the Neoproterozoic-Palaeozoic Hank and Adrar Basins in the south (Villeneuve, 2005). Whereas the fold belts surrounding the West African Craton (Fig. 1) were folded and metamorphosed during the Pan-African and/or Variscan orogenies (e.g. Black *et al.*, 1979; Guiraud *et al.*, 1987; Purdy, 1987; Hoepffner *et al.*, 2005; Gasquet *et al.*, 2008; Soulaimani and Burkhard, 2008), the cratonic basement exposed in the Reguibat and Man-Leo shields (Fig. 1) is

56 considered to have been tectonically stable since 1700 Ma (e.g. Villeneuve and Cornée, 1994).
57 However, recently published apatite fission track and (U-Th)/He analyses on samples from the
58 central and western Reguibat proposed that major post-Triassic cooling/exhumation events
59 affected the shield (Leprêtre *et al.*, 2015; 2017).
60 In this contribution, we present new LTT data from 18 samples collected from the western
61 Reguibat shield, including 17 apatite fission track (AFT), two zircon fission track (ZFT) and seven
62 single-grain apatite (U-Th)/He (AHe) analyses. We compare our results to previously published
63 data (Leprêtre *et al.*, 2014; 2015) and challenge the model of a stable craton by proposing a
64 modified model for the tectonic and thermal evolution of the shield.

65 **Methods and analytical results**

66 Investigation of the thermal history of the western Reguibat basement rocks by AFT, ZFT and AHe
67 analyses allows to constrain the time when the samples passed through the temperature window
68 characteristic of each method: 350—220 °C for ZFT (Yamada *et al.*, 2007), 110—60 °C for AFT
69 (Green *et al.*, 1989), and 75—45 °C (Farley, 2000). Fission track densities, horizontal confined track
70 lengths and Dpar (diameter of etched spontaneous fission tracks, used as a proxy for the chemical
71 composition of apatite) were measured in the apatite grains with internal surfaces parallel to the
72 c-axis (Donelick *et al.*, 1999).
73 Two batches of samples were collected from the exposed magmatic rocks intruding the Archean
74 basement of the western Reguibat Shield (Fig. 2). The first set of samples (AW) was collected along
75 a NW-SE transect, from the syenite, dolerite, and granitoid intrusions outcropping near Awsard
76 (Fig. 2). The second set of samples (MS) was collected along a NNE-SSW transect between Awsard
77 and Tichla (Fig. 2) within the Precambrian granite intrusions. Apart from the syenite intrusions of
78 Awsard which are dated to be ca. 2.46 Ga (Bea *et al.*, 2013), the other sampled intrusions are not

yet dated but are assumed to be Late Archean to Early Palaeoproterozoic (ca. 2.9-1.8 Ga; e.g. Schofield *et al.*, 2012; Jessell *et al.*, 2015).

Age data from this study are presented in Tables 1 and 2. AFT ages range between 74 and 102 Ma for the AW samples, and between 49 and 87 Ma for the MS samples (Table 1). Mean track lengths (MTL) measured in apatite grains vary between 11.8 and 13.3 µm in the AW samples, and between 11.6 and 13.1 µm in the MS samples (Table 1). The measured Dpar values range from 1.69 to 3.08 µm in AW samples, and from 1.72 to 2.95 µm in MS samples (Table 1). ZFT analysis was performed on samples MS-09 and MS-12 and yielded ages of 159 and 118 Ma, respectively (Table 1).

AHe analysis, performed on the samples AW-03, AW-05, and AW-06, yielded uncorrected single-grain ages ranging between 76 and 95 Ma (Table 2). The α-ejection corrected single-grain ages (Farley *et al.*, 1996) vary between 95 and 119 Ma, with single grain ages of the same sample overlapping within 1σ uncertainty (Table 2).

We note that the AHe uncorrected ages are either younger than the AFT ages of the same sample or within the 1σ uncertainty level, while the AHe corrected ages are systematically older than the AFT ages of the same sample. Radiation damage in (old) apatite crystals can cause non-thermal annealing of fissions tracks (e.g. Söderlund *et al.*, 2005; Hendriks and Redfield, 2005) and can increase He retentivity (e.g. Green and Duddy, 2006; Shuster *et al.*, 2006; Flowers, 2009), which may result in an inverted relationship between AHe and AFT ages (i.e. AHe ages older than AFT ages). This is usually associated with a positive correlation between effective uranium concentration (eU) and AHe ages (Fitzgerald *et al.*, 2006; Brown *et al.*, 2013), which is not the case for the Reguibat samples (Table 2). Over-correction for α-ejection, due to U and Th zonation in apatite crystals, could be responsible for the inverted relation between AFT ages and corrected AHe ages observed in our data (Hourigan *et al.*, 2005).

Published thermochronology ages

Leprêtre (2015) and Leprêtre et al. (2014; 2015) presented AFT and AHe analyses on samples from the entire Reguibat Shield (Fig. 1). According to their studies AFT single-grain ages, from the Western Reguibat, range from 108 to 176 Ma, while α-ejection corrected AHe ages range from 14 to 185 Ma. In the central Reguibat, AFT ages vary from 139 to 256 Ma, while α-ejection corrected AHe ages vary from 93 to 149 Ma. In the eastern Reguibat, AFT ages vary from 166 to 497 Ma, while α-ejection corrected AHe ages vary from 40 to 198 Ma. These studies show that the AFT ages get substantially younger westwards, i.e. towards the Atlantic margin.

Overall, AFT ages from Leprêtre et al. (2015) from the western Reguibat are distinctly older than the AFT ages obtained in this study. Even contiguous granitic samples like SC9 and MS-13, which were sampled only 300 m apart, thus are expected to belong to the same intrusive body, produce AFT ages of 143 ± 13 Ma and 57.8 ± 2.7 Ma, respectively. Single-grain AFT data from Leprêtre et al. (2015) reveal a significant spread in individual grain ages, which could be related to variations in apatite chemistry (i.e. chlorine-rich vs. fluorine-rich apatites; see O'Sullivan and Parrish, 1995; Barbarand *et al.*, 2003).

Thermal modelling

We used QTQt software to model the thermal history of the Western Reguibat Shield (Gallagher, 2012). QTQt is based on the Bayesian transdimensional Markov Chain Monte Carlo method (Gilks *et al.*, 1995; Denison *et al.*, 2002) and allows the sampling of a wide range of thermal histories constrained by fission track and (U/Th)He data. The output of the modelling is a collection of time-temperature (t-T) scenarios and other specific t-T paths, such as the maximum likelihood model (i.e. best data-fitting model) and the expected model (i.e. a weighted mean model from the probability distribution of the sampled t-T paths). The fit between the observed and predicted

data is defined by a likelihood function, which quantifies the probability of obtaining the data given by the model. The higher the likelihood log value the better the model fits the data. In addition, the validity of a model must be checked by examining the stability of the log likelihood and the number of t-T points at each iteration. More details about the modelling method are given in Gallagher (2012).

Given the narrow spatial distribution of the samples and the lack of Meso-Cenozoic tectonic structures in the sampled area that could cause varying thermal histories among the samples, we believe that the LTT data illustrate a uniform thermal history and that variation in FT ages are related to compositional changes among the dated apatites (Barbarand *et al.*, 2003; O'Sullivan and Parrish, 1995). Thus, for the purpose of thermal modelling, we combined the AFT data from the six AW samples (Fig. 3a), the AFT data from the eleven MS samples (Fig. 3b), and the ZFT data from MS-09 and MS-12 (Fig. 3c). Due to the range of the LTT ages, we only model the thermal evolution during post-Triassic times (i.e. between 200 and 0 Ma). Initial inverse modelling was carried out to explore several modelling configurations and the modelling sensitivity to He kinetics (Gautheron *et al.*, 2009; Flowers, 2009) and ZFT annealing models (Yamada *et al.*, 2007; Tagami *et al.*, 1988). These initial models are presented in the supplementary file S1. The final QTQt simulation (Fig. 4) uses the He kinetics of Flowers (2009) and the annealing models of Ketchman et al. (2007) and Yamada et al. (2007) for apatite and zircon, respectively. Our test models indicate that changing the ZFT annealing model and the He kinetics have a limited impact on the predicted t-T history (Figs. S4, S5, S6, S8, and S9), however, the He kinetics of Flowers (2009) (Figs. S4, S5, and S6) and the ZFT annealing model of Yamada et al. (2007) (Figs. S8 and S9) best correspond to the observed AHe and ZFT ages, respectively.

The final model (Fig. 4) explores the likelihood of a thermal history that integrates all LTT data, i.e. constrained by ZFT, AFT, and AHe data from both AW and MS samples. The obtained maximum

149 likelihood t-T path is characterized by a major rapid cooling event (-370 °C) during the Early
150 Cretaceous (between 130 and 120 Ma) followed by a thermally unstable period (ca. between 120
151 and 0 Ma) with potentially three additional cooling events of lesser magnitudes during 80—70 Ma
152 (-50 °C), 60—50 Ma (-80 °C), and the Quaternary (-40 °C). The predicted ZFT and AFT ages, along
153 with the predicted track length distributions are consistent with the observed ones (Figs. 4b-c).
154 However, the predicted uncorrected AHe ages are 30 to 60 Ma younger than the observed ones
155 (Fig. 4c). The thermal trend illustrated in this model is fairly similar to the one obtained by Leprêtre
156 et al. (2015) for their samples from the western Reguibat Shield, which predicts three thermal
157 cooling events between the Cretaceous and the present-day (i.e. 130—120 Ma [-120 °C], 90—60
158 Ma [-30 °C], and 10—0 Ma [-50 °C]).

159 **Post-Triassic evolution of the Western Reguibat Shield**

160 LTT data indicate that the western Reguibat Shield shows a differentiated post-Triassic thermal
161 history. Inverse modelling (Fig. 4) suggests a major cooling event during the Early Cretaceous,
162 which brought the sampled basement rocks from mid-crustal to near-surface temperatures,
163 followed by three minor heating events between the Late Cretaceous and the present-day.
164 Heating events occurred during the Aptian—Santonian (120—80 Ma), the Maastrichtian—Early
165 Palaeocene (70—60 Ma), and the Eocene—Pliocene (50—3 Ma).
166 Major magmatic events are recorded in the region, including the Late Triassic-Early Jurassic
167 tholeiitic basalt flows and dikes of the Central Atlantic Magmatic Province (Knight *et al.*, 2004;
168 Marzoli *et al.*, 2004) and the Meso-Cenozoic peri-Atlantic alkaline pulses (Matton and Jébrak,
169 2009). Although volcanic rocks and/or magmatic intrusions related to these magmatic events are
170 yet to be documented in the Reguibat Shield per se, their widespread occurrence along the
171 margins of the Central Atlantic suggests deep mantle or at least asthenosphere origin (Matton
172 and Jébrak, 2009). In addition, the Late Triassic—Early Jurassic rifting in the Central Atlantic

involved major thermal perturbations due to the related lithospheric thinning. Increasing surface heat flux from 40 mWm^{-2} (characteristic of cratonic domains) towards 90 mWm^{-2} (characteristic of rifted domains) can raise the 60 °C isotherm (the upper limit of the AFT partial annealing zone) from a depth of ~5 km to ~2.1 km (Ehlers, 2005). However, seismic data offshore the Dakhla margin indicate that our samples are located 400 to 500 km east of the margin hinge line and that the crust underneath the western Reguibat Shield is at least 27—30 km thick (Labails and Olivet, 2009).

In domains where the crust keeps its integrity through time, large changes in surface heat flow may be accounted for by a change in crustal heat generation only, while variations in basal heat flow from the mantle have a minor impact on the upper portion of the crust (Mareschal and Jaupart, 2004). Thus, the succession of heating and cooling events documented in the western Reguibat Shield by LTT analyses are expected to be largely due to vertical movements of the crust expressed by burial/subsidence and exhumation/erosion, respectively. Given the magnitude of the modelled vertical movements/thermal events, they must be documented in the sedimentary record of the nearby basins of the Atlantic margin. The few published data from the Dakhla margin (Labails and Olivet, 2009), bordering the west Reguibat Shield, do not properly illustrate the stratigraphic architecture of the margin. Well and seismic data from the Tarfaya basin located on the NW margin of the shield, however, show several regressive events (Fig. 5; El Jorfi *et al.*, 2015), certainly associated with, or even driven by, the exhumation of the hinterlands and their erosion. Thus, the Hauterivian—Aptian (130—120 Ma) and the Campanian (80—70 Ma) cooling events correlate with decreases in relative sea level and erosional unconformities in the Tarfaya continental shelf (Fig. 5). The Middle—Late Palaeocene (60—50 Ma) cooling event appears to

coincide with the end of a transgressive phase according to El Jorfi et al. (2015), which persisted through the Eocene and Early Oligocene (Fig. 5; El Jorfi *et al.*, 2015; Gouiza, 2011).

The major cooling event recorded during the Hauterivian—Aptian, which brings the basement rocks from mid-crust to surface temperatures, is consistent with low-temperature thermochronology results from the Anti-Atlas domain in the north (Gouiza *et al.*, 2017; Oukassou *et al.*, 2013; Ruiz *et al.*, 2011). It is also coherent with the presence of Lower Cretaceous sediments unconformably lying on the fringe of the Reguibat basement in the north (Fig. 1), although these sediments have yet to be properly dated.

The heating events on the other hand are attributed to subsidence and basement burial, which means that Mesozoic sediments were deposited on the western Reguibat Shield and later eroded during the following exhumation phases. The eroded sediments were probably routed to the Atlantic shelf and deep basin (Davison, 2005; Gouiza, 2011).

The geological processes driving these thermal events/km-scale vertical movements are unclear, especially since similar vertical movements are documented all along the Moroccan margin (e.g. Ruiz *et al.*, 2011; Ghorbal *et al.*, 2008; Gouiza *et al.*, 2017; Malusà *et al.*, 2007; Oukassou *et al.*, 2013) and the East American conjugate as well (e.g. Roden‐Tice and Tice, 2005; Grist and Zentilli, 2003; Roden‐Tice and Wintsch, 2002). Bertotti and Gouiza (2012) proposed that the Late Jurassic—Early Cretaceous exhumation recorded in the Meseta and the High Atlas are related to coeval regional shortening, documented by syn-sedimentary tectonics in the Essaouira basin. Leprêtre et al. (2017), on the other hand, proposed transient mantle dynamics to account for the major erosional phases recorded on both sides of the Atlantic. Gouiza (2011) investigated the effect of small-scale sublithospheric mantle convection on crustal exhumation, using thermo-mechanical numerical modelling, and showed that surface response to mantle dynamics

underneath continental lithosphere is limited to a few hundreds of metres. However, the numerical modelling did not incorporate erosion, which is known to enhance crustal exhumation. We hypothesise that the major Early Cretaceous exhumation/cooling is driven by a combined action of regional compressional stresses and sublithospheric mantle dynamics. The regional stresses are related to the readjustment of the African plate to the differential opening of the Central, South, and North Atlantics, while mantle dynamics are inherited from the rift system and triggered by the established lateral thermal gradient between thinned and unthinned continental lithosphere (Buck, 1986).

The following cooling events, during the Late Cretaceous, the Palaeocene, and the Quaternary occurred during the Africa-Europe convergence, which began during the Senonian (e.g. Ricou, 1994). Frizon de Lamotte et al. (2009) argue that this convergence was accommodated through time by large wavelength folding/buckling of the African lithosphere during the Late Cretaceous and Palaeocene, and by inversion of the intracontinental rifts (e.g. Atlas rifts) typically during the Middle-Late Eocene and the Plio-Quaternary.

Conclusion

The LTT data indicate that the basement of the western Reguibat Shield experienced a succession of cooling and heating events during Mesozoic and Cenozoic times. According to inverse thermal modelling, a major cooling episode occurred during the Early Cretaceous (130—120 Ma), followed by minor cooling episodes during the Campanian (80—70 Ma), the Middle—Late Palaeocene (60—50 Ma), and the Quaternary (3—0 Ma). These cooling phases are interpreted to be episodes of crustal exhumation, while the heating events are interpreted to reflect subsidence and burial.

The exhumation correlates with regressive events and erosional unconformities documented in well and seismic data form the neighbouring Atlantic basin of Tarfaya.

Since similar exhumation events are recorded in other domains of the Atlantic margin, in Morocco and East North America, we believe that the events are driven by regional processes. The processes are thought to involve a combined action of regional compressional stresses and subcontinental mantle dynamics. The regional stresses are related to plate tectonics and the readjustment of the African plate to the differential opening of the Central, South, and North Atlantics, while mantle dynamics are due to lateral thermal gradients between thinned and unthinned continental lithosphere established during the Atlantic rifting.

Acknowledgements

We are very grateful to the Associate Editor M. Rahn, Prof. J.-P. Liégeois, Prof. D. Frizon de Lamotte, and an anonymous reviewer for their excellent reviews of our manuscript, which helped improve its quality.

References

Barbarand, J., Carter, A., Wood, I. and Hurford, T., 2003. Compositional and structural control of fission-track annealing in apatite: Chemical Geology, **198**, p. 107–137, doi: 10.1016/S0009-2541(02)00424-2.

Bea, F., Montero, P., Haissen, F. and El, A., 2013. 2.46 Ga kalsilite and nepheline syenites from the Awsard pluton, Reguibat Rise of the West African Craton, Morocco. Generation of extremely K-rich magmas at the Archean-Proterozoic transition: Precambrian Research, **224**, p. 242–254, doi: 10.1016/j.precamres.2012.09.024.

Bertotti, G. and Gouiza, M., 2012. Post-rift vertical movements and horizontal deformations in the eastern margin of the Central Atlantic: Middle Jurassic to Early Cretaceous evolution of Morocco: International Journal of Earth Sciences, **101**, p. 2151–2165, doi: 10.1007/s00531-012-0773-4.

Black, R., Caby, R., Moussine-Pouchkine, A., Bayer, R., Bertrand, J.M., Boullier, A.M., Fabre, J. and Lesquer, A., 1979. Evidence for late Precambrian plate tectonics in West Africa: Nature, **278**, p. 223–227, doi: 10.1038/278223a0.

Brown, R.W., Beucher, R., Roper, S., Persano, C., Stuart, F. and Fitzgerald, P., 2013. Natural age dispersion arising from the analysis of broken crystals. Part I: Theoretical basis and implications for the apatite (U–Th)/He thermochronometer: Geochimica et Cosmochimica Acta, **122**, p. 478–497, doi: 10.1016/j.gca.2013.05.041.

Buck, W.R., 1986. Small-scale convection induced by passive rifting: the cause for uplift of rift shoulders: Earth and Planetary Science Letters, **77**, p. 362–372, doi: 10.1016/0012-821X(86)90146-9.

Davison, I., 2005. Central Atlantic margin basins of North West Africa: Geology and hydrocarbon potential (Morocco to Guinea): Journal of African Earth Sciences, **43**, p. 254–274, doi: 10.1016/j.jafrearsci.2005.07.018.

Denison, T.D.G., Holmes, C.C., Mallick, B.K. and Smith, A.F.M., 2002. Bayesian Methods for Nonlinear Classification and Regression: Wiley, Chichester, U. K.

Donelick, R.A., Ketcham, R.A. and Carlson, W.D., 1999. Variability of apatite fission-track annealing kinetics: II. Crystallographic orientation effects: American Mineralogist, **84**, p. 1224–1234.

Ehlers, T.A., 2005. Crustal Thermal Processes and the Interpretation of Thermochronometer Data: Reviews in Mineralogy and Geochemistry, **58**, p. 315–350, doi: 10.2138/rmg.2005.58.12.

El Jorfi, L., Süss, M.P., Aigner, T. and Mhammdi, N., 2015. Triassic – Quaternary Sequence Stratigraphy of the Tarfaya Basin (moroccan Atlantic): Structural

289 Evolution, Eustasy and Sedimentation: Journal of Petroleum Geology, **38**, p. 77–
290 98, doi: 10.1111/jpg.12599.

291 Ennih, N. and Liégeois, J.-P., 2008. The boundaries of the West African craton, with
292 special reference to the basement of the Moroccan metacratonic Anti-Atlas belt:
293 Geological Society, London, Special Publications, **297**, p. 1–17, doi:
294 10.1144/SP297.1.

295 Farley, K.A., 2000. Helium diffusion from apatite: General behavior as illustrated by
296 Durango fluorapatite: Journal of Geophysical Research: Solid Earth, **105**, p. 2903–
297 2914, doi: 10.1029/1999JB900348.

298 Farley, K.A., Wolf, R.A. and Silver, L.T., 1996. The effects of long alpha-stopping
299 distances on (U-Th)/He ages: Geochimica et Cosmochimica Acta, **60**, p. 4223–
300 4229, doi: 10.1016/S0016-7037(96)00193-7.

301 Fitzgerald, P.G., Baldwin, S.L., Webb, L.E. and O'Sullivan, P.B., 2006. Interpretation of
302 (U–Th)/He single grain ages from slowly cooled crustal terranes: A case study from
303 the Transantarctic Mountains of southern Victoria Land: Chemical Geology, **225**,
304 p. 91–120, doi: 10.1016/j.chemgeo.2005.09.001.

305 Flowers, R.M., 2009. Exploiting radiation damage control on apatite (U-Th)/He dates in
306 cratonic regions: Earth and Planetary Science Letters, **277**, p. 148–155, doi:
307 10.1016/j.epsl.2008.10.005.

308 Frizon de Lamotte, D., Andrieux, J. and Guezou, J.C., 1991. Cinématique des
309 chevauchements néogènes dans l'Arc betico-rifain; discussion sur les modèles
310 géodynamiques: Bulletin de la Société Géologique de France, **162**, p. 611–626.

311 Frizon De Lamotte, D., Leturmy, P., Missenard, Y., Khomsi, S., Ruiz, G., Saddiqi, O.,
312 Guillocheau, F. and Michard, A., 2009. Mesozoic and Cenozoic vertical
313 movements in the Atlas system (Algeria, Morocco, Tunisia): An overview:
314 Tectonophysics, **475**, p. 9–28, doi: 10.1016/j.tecto.2008.10.024.

315 Gallagher, K., 2012. Transdimensional inverse thermal history modeling for quantitative
316 thermochronology: Journal of Geophysical Research: Solid Earth, **117**, p. B02408,
317 doi: 10.1029/2011JB008825.

318 Gasquet, D., Ennih, N., Liégeois, J.-P., Soulaimani, A. and Michard, A., 2008. The Pan-
319 African Belt. In: Continental Evolution: The Geology of Morocco (Michard, A.,,
320 Saddiqi, O.,, Chalouan, A., and Frizon de Lamotte, D., eds.) Springer Berlin
321 Heidelberg, Berlin, Heidelberg.

322 Gautheron, C., Tassan-Got, L., Barbarand, J. and Pagel, M., 2009. Effect of alpha-damage
323 annealing on apatite (U–Th)/He thermochronology: Chemical Geology, **266**, p.
324 157–170, doi: 10.1016/j.chemgeo.2009.06.001.

Ghorbal, B., 2009. Mesozoic to Quaternary thermo-tectonic evolution of Morocco (NW Africa) [Ph.D Thesis]: Vrije Universiteit, 231 p.

Ghorbal, B., Bertotti, G., Foeken, J. and Andriessen, P., 2008. Unexpected Jurassic to Neogene vertical movements in 'stable' parts of NW Africa revealed by low temperature geochronology: Terra Nova, **20**, p. 355–363, doi: 10.1111/j.1365-3121.2008.00828.x.

Gilks, W.R., Richardson, S. and Spiegelhalter, D., 1995. Markov Chain Monte Carlo in Practice: Chapman and Hall, London, U.K.

Gouiza, M., 2011. Mesozoic Source-to-Sink Systems in NW Africa: Geology of vertical movements during the birth and growth of the Moroccan rifted margin [Ph.D Thesis]: Vrije Universiteit Amsterdam, 170 p.

Gouiza, M., Charton, R., Bertotti, G., Andriessen, P. and Storms, J.E.A., 2017. Post-Variscan evolution of the Anti-Atlas belt of Morocco constrained from low-temperature geochronology: International Journal of Earth Sciences, **106**, p. 593–616, doi: 10.1007/s00531-016-1325-0.

Green, P.F. and Duddy, I.R., 2006. Interpretation of apatite (U–Th)/He ages and fission track ages from cratons: Earth and Planetary Science Letters, **244**, p. 541–547, doi: 10.1016/j.epsl.2006.02.024.

Green, P.F., Duddy, I.R., Laslett, G.M., Hegarty, K.A., Gleadow, A.J.W. and Lovering, J.F., 1989. Thermal annealing of fission tracks in apatite 4. Quantitative modelling techniques and extension to geological timescales: Chemical Geology: Isotope Geoscience section, **79**, p. 155–182, doi: 10.1016/0168-9622(89)90018-3.

Grist, A.M. and Zentilli, M., 2003. Post-Paleocene cooling in the southern Canadian Atlantic region: evidence from apatite fission track models: Canadian Journal of Earth Sciences, **40**, p. 1279–1297(19).

Guiraud, R., Bellion, Y., Benkhelil, J. and Moreau, C., 1987. Post-Hercynian tectonics in Northern and Western Africa: Geological Journal, **22**, p. 433–466, doi: 10.1002/gj.3350220628.

Hendriks, B.W.H. and Redfield, T.F., 2005. Apatite fission track and (U-Th)/He data from Fennoscandia: An example of underestimation of fission track annealing in apatite: Earth and Planetary Science Letters, **236**, p. 443–458, doi: 10.1016/j.epsl.2005.05.027.

Hoepffner, C., Soulaimani, A. and Piqué, A., 2005. The Moroccan Hercynides: Journal of African Earth Sciences, **43**, p. 144–165, doi: 16/j.jafrearsci.2005.09.002.

Hourigan, J.K., Reiners, P.W. and Brandon, M.T., 2005. U-Th zonation-dependent alpha-ejection in (U-Th)/He chronometry: Geochimica et Cosmochimica Acta, **69**, p. 3349–3365, doi: 10.1016/j.gca.2005.01.024.

Jessell, M., Santoul, J., Baratoux, L., Youbi, N., Ernst, R.E., Metelka, V., Miller, J. and Perrouty, S., 2015. An updated map of West African mafic dykes: Journal of African Earth Sciences, **112**, **Part B**, p. 440–450, doi: 10.1016/j.jafrearsci.2015.01.007.

Ketcham, R.A., Carter, A., Donelick, R.A., Barbarand, J. and Hurford, A.J., 2007. Improved modeling of fission-track annealing in apatite: American Mineralogist, **92**, p. 799–810, doi: 10.2138/am.2007.2281.

Klitgord, K.D., Schouten, H., Vogt, P.R. and Tucholke, B.E., 1986. Plate kinematics of the central Atlantic. In: The Western North Atlantic Region: The Geology of North America Geological Society of America, USA, p. 351–378.

Knight, K.B., Nomade, S., Renne, P.R., Marzoli, A., Bertrand, H. and Youbi, N., 2004. The Central Atlantic Magmatic Province at the Triassic-Jurassic boundary: paleomagnetic and 40Ar/39Ar evidence from Morocco for brief, episodic volcanism: Earth and Planetary Science Letters, **228**, p. 143–160, doi: 10.1016/j.epsl.2004.09.022.

Labails, C. and Olivet, J.-L., 2009. Crustal structure of the SW Moroccan margin from wide-angle and reflection seismic data (the Dakhla experiment). Part B -- The tectonic heritage: Tectonophysics, **468**, p. 83–97, doi: 10.1016/j.tecto.2008.08.028.

Lécorché, J.P., Roussel, J., Sougy, J. and Guetat, Z., 1983. An interpretation of the geology of the Mauritanides orogenic belt (West Africa) in the light of geophysical data: Geological Society of America Memoirs, **158**, p. 131–148, doi: 10.1130/MEM158-p131.

Leprêtre, R., 2015. Evolution phanérozoïque du Craton Ouest Africain et de ses bordures Nord et Ouest [Ph.D Thesis]: Université Paris Sud - Paris XI, 898 p.

Leprêtre, R., Barbarand, J., Missenard, Y., Gautheron, C., Pinna-Jamme, R. and Saddiqi, O., 2017. Mesozoic evolution of NW Africa: implications for the Central Atlantic Ocean dynamics: Journal of the Geological Society,, p. jgs2016-100, doi: 10.1144/jgs2016-100.

Leprêtre, R., Barbarand, J., Missenard, Y., Leparmentier, F. and Frizon De Lamotte, D., 2014. Vertical movements along the northern border of the West African Craton: the Reguibat Shield and adjacent basins: Geological Magazine, **151**, p. 885–898, doi: 10.1017/S0016756813000939.

Leprêtre, R., Missenard, Y., Barbarand, J., Gautheron, C., Saddiqi, O. and Pinna-Jamme, R., 2015. Postrift history of the eastern central Atlantic passive margin: Insights from the Saharan region of South Morocco: Journal of Geophysical Research: Solid Earth, **120**, p. 2014JB011549, doi: 10.1002/2014JB011549.

Malusà, M.G., Polino, R., Feroni, A.C., Ellero, A., Ottria, G., Baidder, L. and Musumeci, G., 2007. Post-Variscan tectonics in eastern Anti-Atlas (Morocco): Terra Nova, **19**, p. 481–489, doi: 10.1111/j.1365-3121.2007.00775.x.

Mareschal, J.C. and Jaupart, C., 2004. Variations of surface heat flow and lithospheric thermal structure beneath the North American craton: Earth and Planetary Science Letters, **223**, p. 65–77, doi: 10.1016/j.epsl.2004.04.002.

Martínez-Loriente, S., Sallarès, V., Gràcia, E., Bartolome, R., Dañobeitia, J.J. and Zitellini, N., 2014. Seismic and gravity constraints on the nature of the basement in the Africa-Eurasia plate boundary: New insights for the geodynamic evolution of the SW Iberian margin: Journal of Geophysical Research: Solid Earth, **119**, p. 2013JB010476, doi: 10.1002/2013JB010476.

Marzoli, A., Bertrand, H., Knight, K.B., Cirilli, S., Buratti, N., Vérati, C., Nomade, S., Renne, P.R., Youbi, N., Martini, R., Allenbach, K., Neuwerth, R., Rapaille, C., Zaninetti, L. and Bellieni, G., 2004. Synchrony of the Central Atlantic magmatic province and the Triassic-Jurassic boundary climatic and biotic crisis: Geology, **32**, p. 973–976, doi: 10.1130/G20652.1.

Matton, G. and Jébrak, M., 2009. The Cretaceous Peri-Atlantic Alkaline Pulse (PAAP): Deep mantle plume origin or shallow lithospheric break-up? Tectonophysics, **469**, p. 1–12, doi: 10.1016/j.tecto.2009.01.001.

O'Sullivan, P.B. and Parrish, R.R., 1995. The importance of apatite composition and single-grain ages when interpreting fission track data from plutonic rocks: a case study from the Coast Ranges, British Columbia: Earth and Planetary Science Letters, **132**, p. 213–224, doi: 10.1016/0012-821X(95)00058-K.

Oukassou, M., Saddiqi, O., Barbarand, J., Sebti, S., Baidder, L. and Michard, A., 2013. Post-Variscan exhumation of the Central Anti-Atlas (Morocco) constrained by zircon and apatite fission-track thermochronology: Terra Nova, **25**, p. 151–159, doi: 10.1111/ter.12019.

Piqué, A., Tricart, P., Guiraud, R., Laville, E., Bouaziz, S., Amrhar, M. and Ait Ouali, R., 2002. The Mesozoic-Cenozoic Atlas belt (North Africa): an overview: Geodinamica Acta, **15**, p. 185–208, doi: 10.1016/S0985-3111(02)01088-4.

Purdy, G.M., 1987. Regional trends in the geology of the Appalachian-Caledonian-Hercynian-Mauritanide orogen: Earth-Science Reviews, **24**, p. 279–280, doi: 10.1016/0012-8252(87)90063-8.

Ricou, L.-E., 1994. Tethys reconstructed : plates, continental fragments and their Boundaries since 260 Ma from Central America to South-eastern Asia.: Geodinamica Acta, **7**, p. 169–218, doi: 10.1080/09853111.1994.11105266.

Roden-Tice, M.K. and Tice, S.J., 2005. Regional-Scale Mid-Jurassic to Late Cretaceous Unroofing from the Adirondack Mountains through Central New England Based

on Apatite Fission-Track and (U-Th)/He Thermochronology: The Journal of Geology, **113**, p. 535–552.

Roden-Tice, M.K. and Wintsch, R.P., 2002. Early Cretaceous Normal Faulting in Southern New England: Evidence from Apatite and Zircon Fission-Track Ages: The Journal of Geology, **110**, p. 159–178.

Ruiz, G.M.H., Sebti, S., Negro, F., Saddiqi, O., Frizon de Lamotte, D., Stockli, D., Foeken, J., Stuart, F., Barbarand, J. and Schaer, J.-P., 2011. From central Atlantic continental rift to Neogene uplift - western Anti-Atlas (Morocco): Terra Nova, **23**, p. 35–41, doi: 10.1111/j.1365-3121.2010.00980.x.

Saddiqi, O., El Haimer, F.-Z., Michard, A., Barbarand, J., Ruiz, G.M.H., Mansour, E.M., Leturmy, P. and Frizon de Lamotte, D., 2009. Apatite fission-track analyses on basement granites from south-western Meseta, Morocco: Paleogeographic implications and interpretation of AFT age discrepancies: Tectonophysics, **475**, p. 29–37, doi: 10.1016/j.tecto.2009.01.007.

Schofield, D.I., Horstwood, M.S.A., Pitfield, P.E.J., Gillespie, M., Darbyshire, F., O'Connor, E.A. and Abdouloye, T.B., 2012. U–Pb dating and Sm–Nd isotopic analysis of granitic rocks from the Tiris Complex: New constaints on key events in the evolution of the Reguibat Shield, Mauritania: Precambrian Research, **204**–**205**, p. 1–11, doi: 10.1016/j.precamres.2011.12.008.

Sebti, S., Saddiqi, O., El Haimer, F.Z., Michard, A., Ruiz, G., Bousquet, R., Baidder, L. and Frizon de Lamotte, D., 2009. Vertical movements at the fringe of the West African Craton: First zircon fission track datings from the Anti-Atlas Precambrian basement, Morocco: Comptes Rendus Geosciences, **341**, p. 71–77, doi: 10.1016/j.crte.2008.11.006.

Sehrt, M., 2014. Variscan to Neogene long-term landscape evolution at the Moroccan passive continental margin (Tarfaya Basin and western Anti-Atlas) [Ph.D Thesis]: Heidelberg, 152 p.

Shuster, D.L., Flowers, R.M. and Farley, K.A., 2006. The influence of natural radiation damage on helium diffusion kinetics in apatite: Earth and Planetary Science Letters, **249**, p. 148–161, doi: 10.1016/j.epsl.2006.07.028.

Söderlund, P., Juez-Larré, J., Page, L.M. and Dunai, T.J., 2005. Extending the time range of apatite (U-Th)/He thermochronometry in slowly cooled terranes: Palaeozoic to Cenozoic exhumation history of southeast Sweden: Earth and Planetary Science Letters, **239**, p. 266–275, doi: 10.1016/j.epsl.2005.09.009.

Soulaimani, A. and Burkhard, M., 2008. The Anti-Atlas chain (Morocco): the southern margin of the Variscan belt along the edge of the West African craton: Geological Society, London, Special Publications, **297**, p. 433–452, doi: 10.1144/SP297.20.

473 Tagami, T., Lal, N., Sorkhabi, R.B., Ito, H. and Nishimura, S., 1988. Fission track dating
474 using external detector method: Memoirs of the Faculty of Science, Kyoto
475 University, Series of Geology and Mineralogy, **53**, p. 1–30.

476 Teixell, A., Bertotti, G., Frizon de Lamotte, D. and Charroud, M., 2009. The geology of
477 vertical movements of the lithosphere: An overview: Tectonophysics, **475**, p. 1–8,
478 doi: 10.1016/j.tecto.2009.08.018.

479 Torsvik, T.H., Rousse, S., Labails, C. and Smethurst, M.A., 2009. A new scheme for the
480 opening of the South Atlantic Ocean and the dissection of an Aptian salt basin:
481 Geophysical Journal International, **177**, p. 1315–1333, doi: 10.1111/j.1365-
482 246X.2009.04137.x.

483 Villeneuve, M., 2005. Paleozoic basins in West Africa and the Mauritanide thrust belt:
484 Journal of African Earth Sciences, **43**, p. 166–195, doi: 16/j.jafrearsci.2005.07.012.

485 Villeneuve, M. and Cornée, J.J., 1994. Structure, evolution and palaeogeography of the
486 West African craton and bordering belts during the Neoproterozoic: Precambrian
487 Research, **69**, p. 307–326, doi: 16/0301-9268(94)90094-9.

488 Whiteman, A.J., 1965. The geological map of Africa, scale 1:5,000,000, new edition 1963:
489 Geological Magazine, **102**, p. 80–86.

490 Yamada, R., Murakami, M. and Tagami, T., 2007. Statistical modelling of annealing
491 kinetics of fission tracks in zircon; Reassessment of laboratory experiments:
492 Chemical Geology, **236**, p. 75–91, doi: 10.1016/j.chemgeo.2006.09.002.

Figure captions

1. Simplified geological map of (a) the West African Craton (WAC) and (b) the Reguibat Shield and surrounding domains (modified from the geological map of Africa 1:5,000,000 (Whiteman, 1965) and after Ennih and Liégeois (2008)). Red dots with white circle indicate the location of samples analysed in this study, yellow dots with black circle indicate the location of samples analysed by Leprêtre (2015) and Leprêtre et al. (2014; 2015).
2. Zoom-in on the Western Reguibat Shield showing in details the location of samples analysed in this study (red dots) and by Leprêtre et al. (2015) (Black dots). MS samples are marked with orange circles, AW samples with purple circles. Same legend for geological units as in Figure 1.
3. Radial plots of single grain AFT ages from a) AW samples and b) MS samples, and single grain ZFT ages from c) MS-09 and MS-12.
4. Thermal inverse modelling results constrained by ZFT, AFT, and AHe data from the combined AW and MS samples. a) Maximum Likelihood and expected t-T paths, and probability distribution of sampled thermal histories. b) Observed and predicted apatite mean track length distributions. c) Observed and predicted ZFT, AFT, and AHe ages.
5. Chronostratigraphic chart of the Tarfaya basin showing the sedimentary gaps and seismic sequences (El Jorfi *et al.*, 2015) with respect to the maximum likelihood t-T path obtained from the thermal modelling and the regional tectonic events [a: Central Atlantic Rift (Klitgord *et al.*, 1986); b: South Atlantic Rift (Torsvik *et al.*, 2009); c: Africa-Iberia collision (Martínez-Loriente *et al.*, 2014); d: Rif-Atlas orogeny (Frizon de Lamotte *et al.*, 1991; Piqué *et al.*, 2002)].

Table captions

1. Analytical results of apatite fission track analyses of the samples collected from the Moroccan Reguibat Shield. Errors are ± 1σ, calculated using the Zeta calibration technique (ζ_{AFT} = 335 ± 22 for AW samples; ζ_{AFT} = 358 ± 10 and ζ_{ZFT} = 128 ± 3 for MS samples). ρ_s and ρ_i are the spontaneous and induced track densities, respectively; N_i and N_s are the numbers of spontaneous and induced tracks, respectively. For samples passing the $P(\chi^2) > 5$ %, pooled ages were calculated. For AW-02 ($P(\chi^2)$ = 2.42%) a central age was calculated. ρ_d = 0.80532×10^6 tr/cm^2 (N_d = 16627) for AW samples. For MS samples: ρ_d = 1.0537×10^6 tr/cm^2 (N_d = 21755) for AFT and ρ_d = 0.47194×10^6 tr/cm^2 (N_d = 9744) for ZFT.
2. Analytical results of apatite (U-Th)/He analyses of AW samples. Uncorrected and α-ejection corrected ages (= uncorrected age / F_t) are shown. Errors are calculated by adding errors from the analytical procedure, the crystal size and on the variability of the Durango standard measured. α-ejection correction is calculated to account for alpha loss in the outer 20 µm of the apatite crystal (Farley *et al.*, 1996).

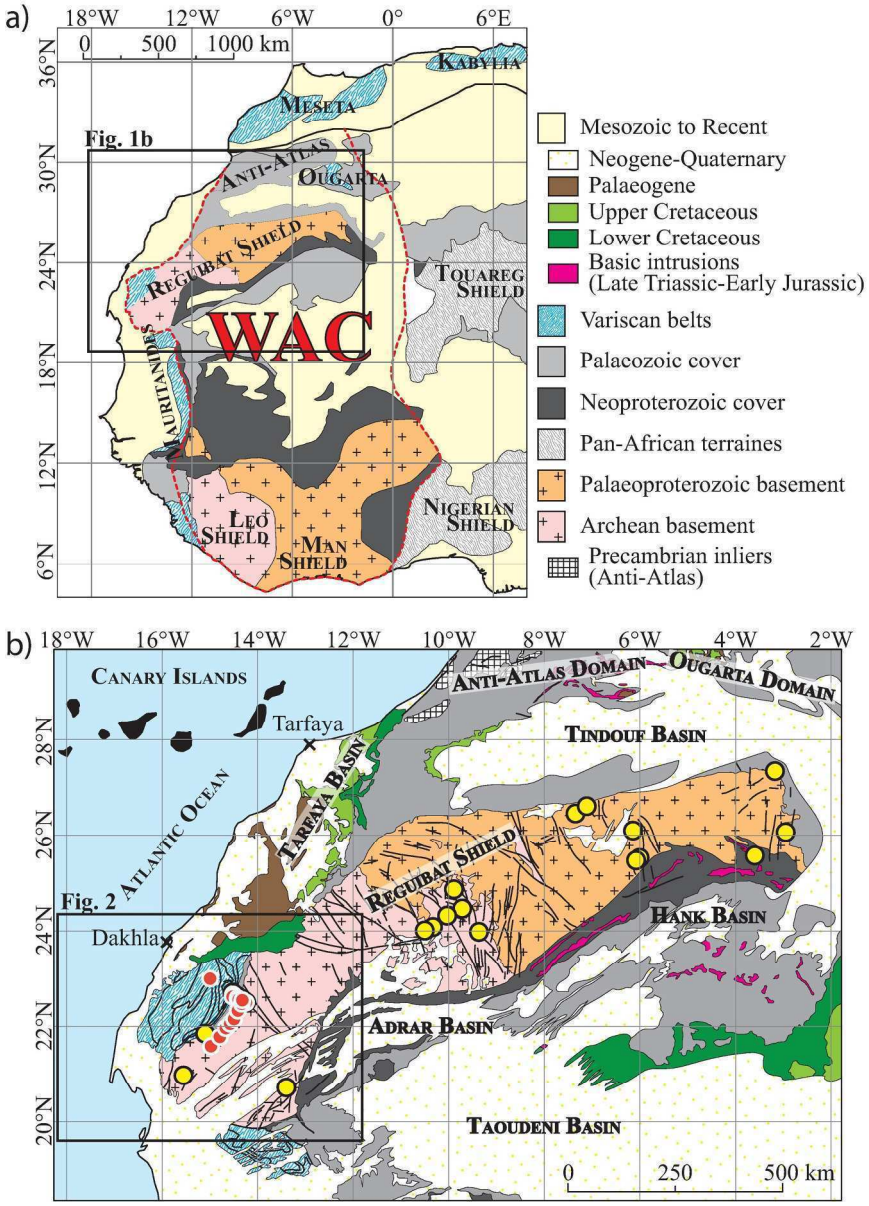

Simplified geological map of (a) the West African Craton (WAC) and (b) the Reguibat Shield and surrounding domains (modified from the geological map of Africa 1:5,000,000 (Whiteman, 1965) and after Ennih and Liégeois (2008)). Red dots with white circle indicate the location of samples analysed in this study, yellow dots with black circle indicate the location of samples analysed by Leprêtre (2015) and Leprêtre et al. (2014; 2015).

179x249mm (300 x 300 DPI)

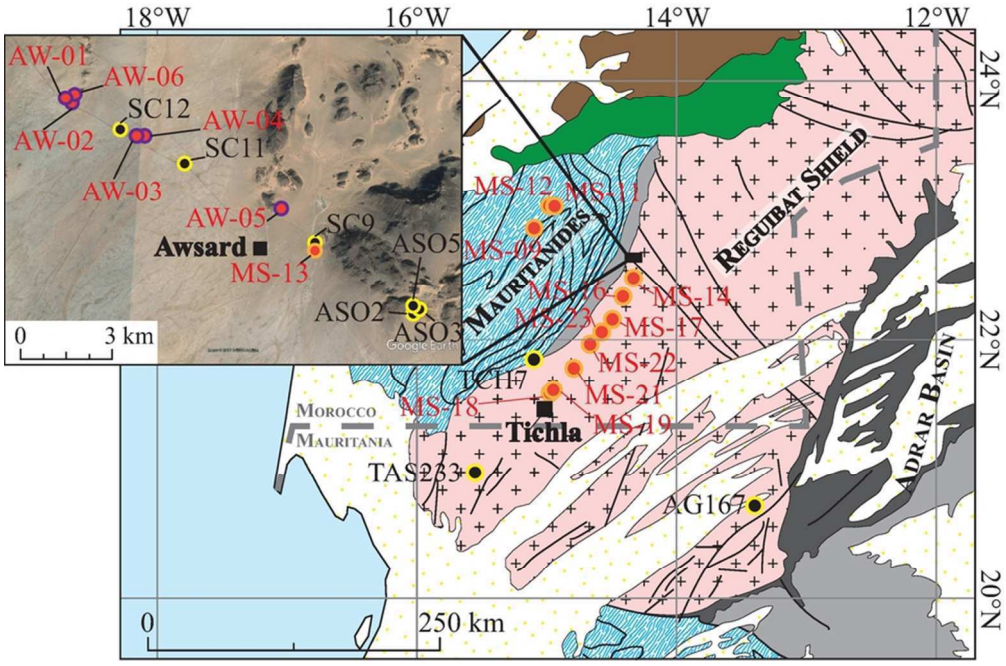

Zoom-in on the Western Reguibat Shield showing in details the location of samples analysed in this study (red dots) and by Leprêtre et al. (2015) (Black dots). MS samples are marked with orange circles, AW samples with purple circles. Same legend for geological units as in Figure 1.

81x53mm (300 x 300 DPI)

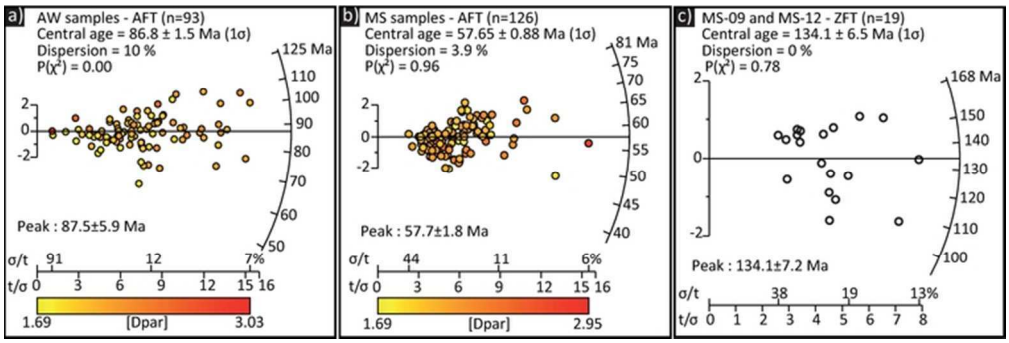

Radial plots of single grain AFT ages from a) AW samples and b) MS samples, and single grain ZFT ages from c) MS-09 and MS-12.

64x21mm (300 x 300 DPI)

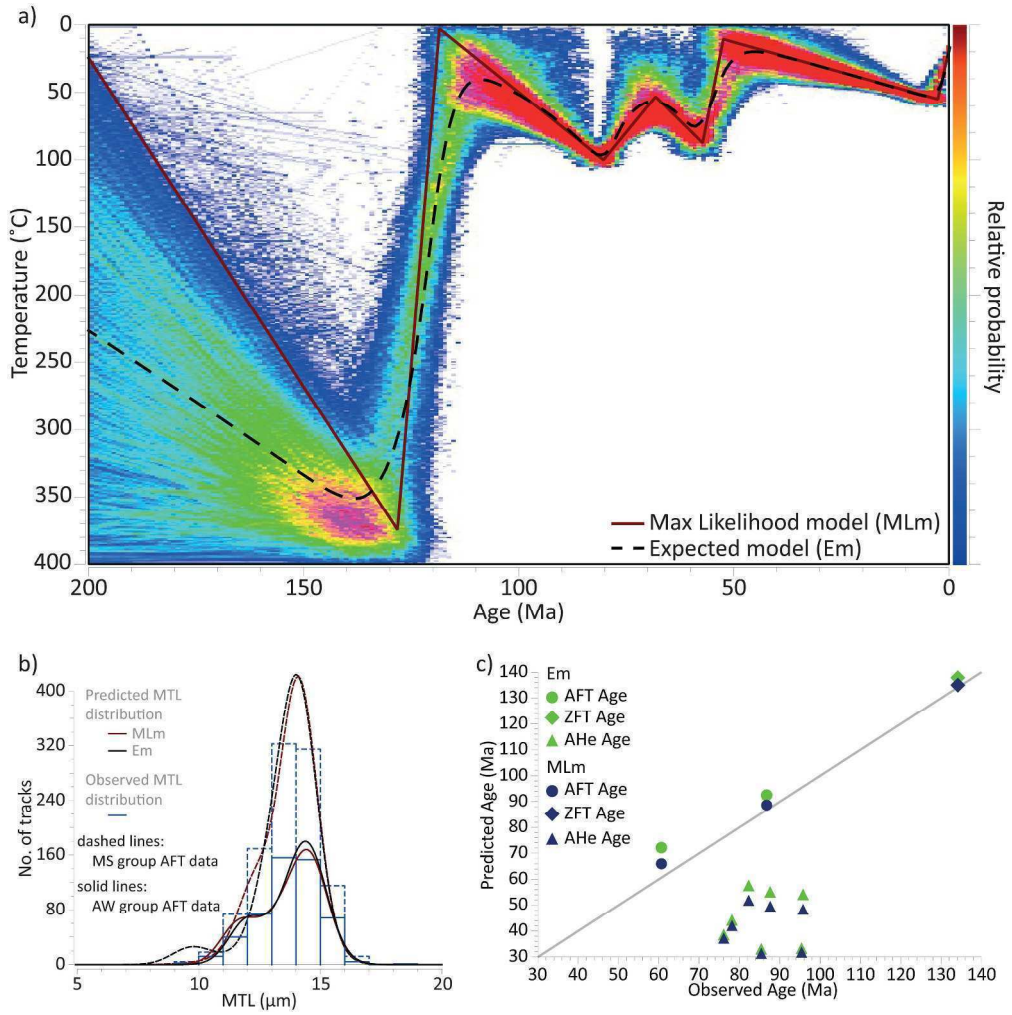

Thermal inverse modelling results constrained by ZFT, AFT, and AHe data from the combined AW and MS samples. a) Maximum Likelihood and expected t-T paths, and probability distribution of sampled thermal histories. b) Observed and predicted apatite mean track length distributions. c) Observed and predicted ZFT, AFT, and AHe ages.

259x261mm (300 x 300 DPI)

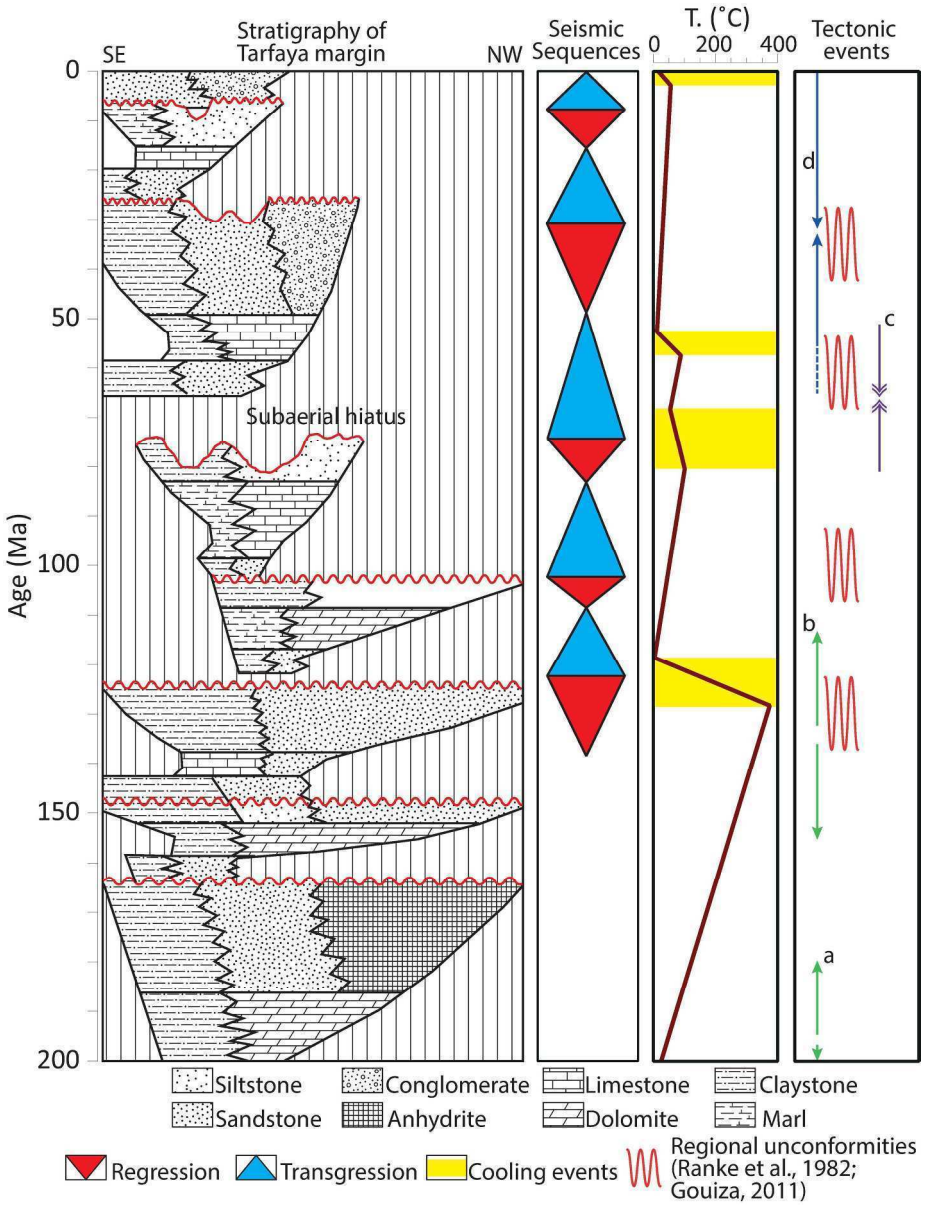

Chronostratigraphic chart of the Tarfaya basin showing the sedimentary gaps and seismic sequences (El Jorfi et al., 2015) with respect to the maximum likelihood t-T path obtained from the thermal modelling and the regional tectonic events [a: Central Atlantic Rift (Klitgord et al., 1986); b: South Atlantic Rift (Torsvik et al., 2009); c: Africa-Iberia collision (Martínez-Loriente et al., 2014); d: Rif-Atlas orogeny (Frizon de Lamotte et al., 1991; Piqué et al., 2002)].

210x275mm (300 x 300 DPI)

Sample	Coordinates	Elevation (m)	Rock type	Mineral	Number of grains	ρ_s 10^6 tr/cm^2 (N_s)	ρ_i 10^6 tr/cm^2 (N_i)	P(χ^2) (%)	Fission track age (Ma)	Mean track length (µm) (# measured lengths)	min-max Dpar (µm) (# measured Dpar)
AW-01	N22°35'46.05" W14°24'04.40"	302	Granitoid	apatite	21	1.2728 (1630)	2.0287 (2598)	44.94	83.8 ± 6.2	11.77 ± 0.19 (101)	1.76-2.30 (21)
AW-02	N22°35'50.09" W14°24'01.21"	310	Syenite	apatite	17	1.1599 (1893)	2.0711 (3380)	2.42	74.0 ± 5.8	12.71 ± 0.15 (101)	1.69-2.26 (17)
AW-03	N22°35'01.15" W14°22'28.41"	290	Doleritic dyke	apatite	20	0.7107 (1340)	1.1016 (2077)	91.21	86.2 ± 6.5	11.76 ± 0.24(59)	1.782-2.255 (20)
AW-04	N22°35'01.57" W14°22'36.38"	290	Doleritic dyke	apatite	9	1.1753 (510)	1.6339 (709)	91.62	95.4 ± 8.4	13.29 ± 0.47 (18)	1.81-3.03 (8)
AW-05	N22°33'41.75" W14°19'31.38"	320	Syenite	apatite	12	1.9688 (2268)	3.0451 (3508)	95.93	86.4 ± 6.2	12.71 ± 0.15 (111)	1.88-2.32 (12)
AW-06	N22°35'47.39" W14°24'03.18"	315	Syenite	apatite	15	1.9419 (2692)	2.5472 (3531)	54.77	101.7 ± 7.2	12.80 ± 0.12 (120)	1.87-2.31 (15)
MS-09	N22°51'45.71" W15°05'50.82"	191	Granite	zircon	10	9.599 (1115)	1.799 (209)	100	159.2 ± 12.7		
MS-11	N23°01'6.74" W15°00'04.15"	222	Granite	apatite	15	0.0889 (124)	0.2522 (352)	100	66.1 ± 7.2	12.30 ± 0.33 (8)	1.79-2.35 (75)
MS-12	N23°01'9.32" W15°00'14.45"	218	Granite	apatite	11	1.9425 (2094)	4.1837 (4510)	98.9	87.0 ± 3.4	12.37 ± 0.1 (210)	1.82-2.19 (56)
				zircon	9	10.341 (1241)	2.633 (316)	92.7	117.5 ± 8.0		
MS-13	N22°32'57.96" W14°18'53.40"	310	Granite	apatite	12	0.9524 (967)	3.0957 (3143)	98.1	57.8 ± 2.7	12.29 ± 0.16 (102)	1.86-2.79 (60)
MS-14	N22°29'44.27" W14°19'47.95"	277	Granite	apatite	15	0.2586 (370)	0.9841 (1408)	99.9	49.4 ± 3.2	13.13 ± 0.14 (96)	1.96-2.66 (75)
MS-16	N22°22'44.24" W14°32'03.27"	271	Granite	apatite	10	0.6745 (661)	2.5765 (2525)	95.4	49.2 ± 2.6	12.75 ± 0.14 (108)	1.85-2.46 (51)
MS-17	N22°11'38.69" W14°28'57.23"	266	Granite	apatite	10	0.8455 (696)	2.4514 (2018)	94	64.7 ± 3.4	12.39 ± 0.15 (90)	1.72-2.95 (50)
MS-18	N22°05'01.88" W14°34'38.63"	176	Granite	apatite	15	0.2259 (321)	0.7241 (1029)	100	58.6 ± 4.1	12.15 ± 0.27 (38)	1.74-2.14 (75)
MS-19	N22°00'31.50" W14°39'05.23"	177	Granite	apatite	15	0.2986 (439)	0.9762 (1435)	100	57.4 ± 3.4	12.22 ± 0.23 (61)	1.69-2.28 (75)
MS-21	N21°47'35.28" W14°48'03.66"	212	Granite	apatite	19	0.2684 (483)	1.1116 (2000)	100	45.4 ± 2.6	11.63 ± 0.18 (100)	1.92-2.28 (90)
MS-22	N21°36'04.96" W14°57'42.34"	245	Granite	apatite	15	0.878 (1206)	2.5924 (3567)	99.6	63.6 ± 2.8	12.11 ± 0.19 (112)	1.75-2.29 (75)
MS-23	N21°35'57.63" W14°57'52.82"	240	Granite	apatite	15	0.6279 (923)	1.7925 (2635)	93.8	65.7 ± 3.1	12.12 ± 0.16 (102)	1.77-2.10 (77)

Sample	Coordinates	Crystal length (µm)	Crystal radius (µm)	Mass (µg)	4He (ncc/gm)	238U (ppm)	232Th (ppm)	Th/U	eU (ppm)	Uncorrected AHe age (Ma)	Error	Ft factor	Corrected AHe age (Ma)	Error
AW-03-I	N22°35'0.24" W 14°22'33.52"	247	76	7.60	1.25E+05	6.71	17.15	2.55	10.74	94.6	8.9	0.80	118.8	11.2
AW-03-III		250	76	8.61	1.38E+05	10.13	20.26	2.00	14.90	75.5	7.5	0.80	94.5	9.3
AW-05-I	N22°33'41.86" W14°19'36.51"	215	62	8.04	3.06E+05	31.01	5.06	0.16	32.20	80.1	7.5	0.77	103.8	9.8
AW-05-III		234	64	7.42	8.07E+05	71.19	19.09	0.27	75.67	87.0	8.2	0.78	111.7	10.5
AW-06-I	N22°35'47.42" W14°24'4.83"	328	86	15.76	8.75E+04	7.97	1.91	0.24	8.42	84.9	8.4	0.84	101.6	10.1
AW-06-II		237	86	29.51	6.48E+05	61.47	13.86	0.23	64.73	81.7	8.1	0.82	99.1	9.8
AW-06-III		193	80	7.78	6.64E+05	53.74	13.50	0.25	56.91	95.1	9.0	0.81	118.0	11.1
Dur11					2.67E+05	11.37	216.93	19.08	62.35	35.1	3.3			
Dur12					2.62E+05	9.37	217.62	23.22	60.51	35.5	3.3			

What follows is supplementary material,

which will be made available online but

will not appear in the print version.

Supporting information for:

Mesozoic and Cenozoic thermal history of the western Reguibat Shield (West African Craton)

Mohamed Gouiza[1], Giovanni Bertotti[2], Paul A. M. Andriessen[3]

[1] University of Leeds, School of Earth and Environment, Leeds LS29JT, UK

[2] TU Delft, Faculty of Civil Engineering and Geosciences, Delft 2628CN, Netherlands

[3] VU University Amsterdam, Faculty of Earth Sciences, Amsterdam 181HV, Netherlands

Introduction

This document contains details about the analytical methods and the initial inverse thermal modelling that was conducted with the QTQt software (Gallagher, 2012) to test various modelling scenarios and examine the sensitivity of the low-temperature thermochronology data from the Western Reguibat Shield.

As a reminder, we grouped the individual AHe, AFT, and ZFT data into two groups, AW and MS, based on the lithology of the samples. AW group combines the AFT and AHe data from the syenite samples AW-01, AW-02, AW-03, AW-04, AW-05, and AW-06. MS group comprises the AFT data from the granite samples MS-11 to MS-23 and the ZFT data from MS-09 and MS-12.

All the inverse simulations presented below use the apatite annealing model of Ketcham et al. (2007), the same inverse modelling prior (Fig. S1), and the same MCMC (Markov chain Monte Carlo) parameters (Fig. S2).

Analytical methods

Fission track ages were obtained using the external detector method (Gleadow and Duddy, 1981) and the samples were sent to the FRM II research reactor in Garching (Germany) for irradiation, along with dosimeter glasses, CN-5 for apatite and CN1 for zircon, of known uranium content for the determination of the thermal neutron flux. Fission track densities, horizontal confined track lengths and Dpar (diameter of etched spontaneous fission tracks) were measured in the apatite grains with internal surfaces parallel to the C-axis with a 100x dry objective and the FTStage 4 upgrade program (Dumitru, 1993). Dpar is used as a proxy for the chemical composition of apatite and therefore for the annealing properties (Donelick *et al.*, 1999). Fission track ages have been calculated with TRACKKEY software (Dunkl, 2002), using zeta values of 334.5 ± 22 and 358 ± 10 for the apatites of the AW and MS sample sets respectively, and a zeta value of 128 ± 3 for the zircons. (U/Th)He dating was accomplished at

the noble gas laboratory of the VU University of Amsterdam. It is a two-step process that involves Helium extraction and the determination of U and Th concentrations using ICP-MS technique. Refer to Gouiza et al. (2017) for more details about the fission track and the (U-Th)/He laboratory procedures.

Sensitivity modelling

AW group

The AW group was first modelled using AFT data (Scenario 1; Fig. S3), then using AFT and AHe data (Scenarios 2 to 4, Figs S4, S5, and S6, respectively). Figures S4, S5, and S6 show the modelling results of simulations adopting no He kinetics (Scenario 2), the He kinetics of Gautheron et al. (2009) (Scenario 3), and the He kinetics of Flowers et al. (2009) (Scenario 4), respectively.

Scenario 1 (Fig. S3) shows a simple thermal history characterized by a prolonged thermal cooling between 130 and 20 Ma, with an initial high cooling rate phase (4 °C/Myr; 130—115 Ma) and a slow cooling rate phase thereafter (0.5 °C/Myr; 115—20 Ma).

Scenarios 2 to 4 show thermal histories characterized by comparable thermal trends with two heating events between 10 and 80 Ma, and between 10 and 0 Ma. Scenario 4 (Fig. S6), using the He Kinetics of Flowers et al. (2009), shows a more stable solution with high number of T(t) points per iteration (7—20) (Fig. S6c) and better predictions of the AHe ages (Fig. S6b).

MS group

The MS group was first modelled using AFT data (Scenario 5; Fig. S7), then using AFT and ZFT data (Scenarios 6 and 7; Figs S8 and S9, respectively). Figures S8 and S9 show the modelling results of simulations adopting the zircon annealing model of Yamada et al. (2007) and of Tagami et al. (1988), respectively.

The maximum likelihood model, obtained in Scenario 5, show two cooling events (Fig. S7a) between 120 and 10 Ma, and near the present-day. The first cooling event occurs in three phases of varying cooling rates: 2 °C/Myr (120—80 Ma), 0.8 °C/Myr (80—30 Ma), and 1.5 °C/Myr (30—10 Ma). The second cooling event is almost instantaneous with a very high cooling rate (50 °C/Myr).

Scenarios 6 and 7 yield comparable thermal histories with a major cooling event (~340 °C) between 140 and 5 Ma and a very minor cooling event (~40 °C) around the present-day (Figs S8 and S9). Both scenarios show a good fit between predicted and observed AFT and ZFT ages (Figs S8b and S9b). However, scenario 6 assuming the ZFT annealing model of Yamada et al. (2007) shows a more stable solutions (Figs S8c and S9c).

References

Donelick, R.A., Ketcham, R.A. and Carlson, W.D., 1999. Variability of apatite fission-track annealing kinetics: II. Crystallographic orientation effects: *American Mineralogist*, **84**, p. 1224–1234.

Dumitru, T.A., 1993. A new computer-automated microscope stage system for fission-track analysis: *Nuclear Tracks and Radiation Measurements*, **21**, p. 575–580, doi: 10.1016/1359-0189(93)90198-I.

Dunkl, I., 2002. Trackkey: a Windows program for calculation and graphical presentation of fission track data: *Computers & Geosciences*, **28**, p. 3–12, doi: 10.1016/S0098-3004(01)00024-3.

Flowers, R.M., 2009. Exploiting radiation damage control on apatite (U-Th)/He dates in cratonic regions: *Earth and Planetary Science Letters*, **277**, p. 148–155, doi: 10.1016/j.epsl.2008.10.005.

Gallagher, K., 2012. Transdimensional inverse thermal history modeling for quantitative thermochronology: *Journal of Geophysical Research: Solid Earth*, **117**, p. B02408, doi: 10.1029/2011JB008825.

Gautheron, C., Tassan-Got, L., Barbarand, J. and Pagel, M., 2009. Effect of alpha-damage annealing on apatite (U–Th)/He thermochronology: *Chemical Geology*, **266**, p. 157–170, doi: 10.1016/j.chemgeo.2009.06.001.

Gleadow, A.J.W. and Duddy, I.R., 1981. A natural long-term track annealing experiment for apatite: *Nuclear Tracks*, **5**, p. 169–174, doi: 10.1016/0191-278X(81)90039-1.

Gouiza, M., Charton, R., Bertotti, G., Andriessen, P. and Storms, J.E.A., 2017. Post-Variscan evolution of the Anti-Atlas belt of Morocco constrained from low-temperature geochronology: *International Journal of Earth Sciences*, **106**, p. 593–616, doi: 10.1007/s00531-016-1325-0.

Ketcham, R.A., Carter, A., Donelick, R.A., Barbarand, J. and Hurford, A.J., 2007. Improved modeling of fission-track annealing in apatite: *American Mineralogist*, **92**, p. 799–810, doi: 10.2138/am.2007.2281.

Tagami, T., Lal, N., Sorkhabi, R.B., Ito, H. and Nishimura, S., 1988. Fission track dating using external detector method: *Memoirs of the Faculty of Science, Kyoto University, Series of Geology and Mineralogy*, **53**, p. 1–30.

Yamada, R., Murakami, M. and Tagami, T., 2007. Statistical modelling of annealing kinetics of fission tracks in zircon; Reassessment of laboratory experiments: *Chemical Geology*, **236**, p. 75–91, doi: 10.1016/j.chemgeo.2006.09.002.

a)

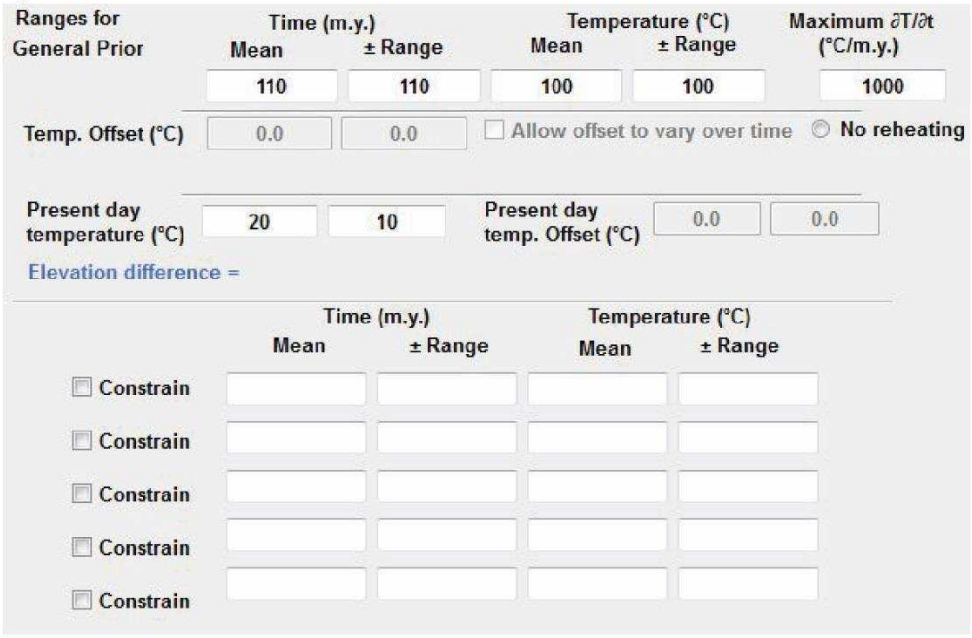

b)

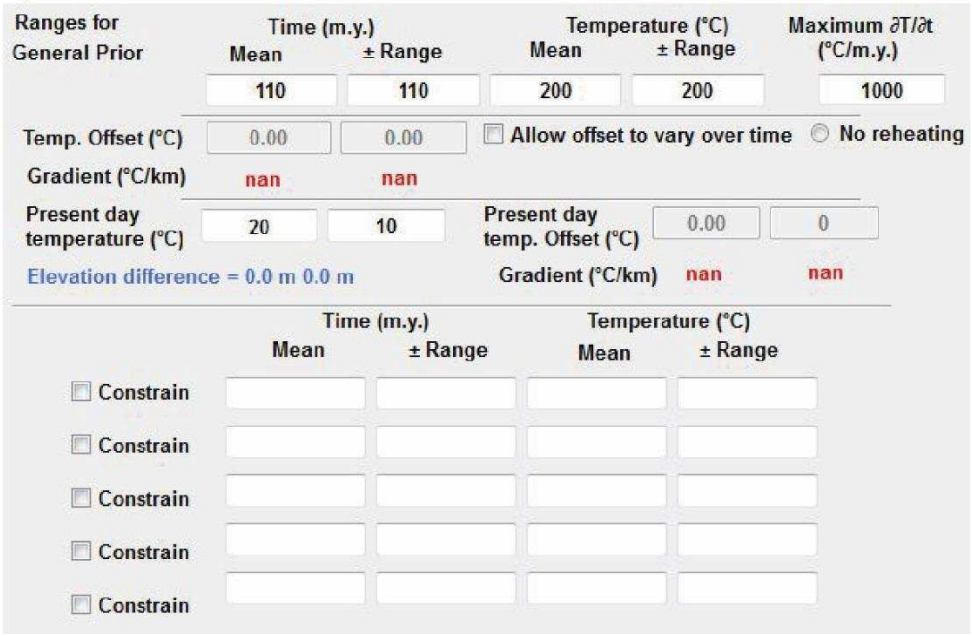

Fig. S1 – Inverse modelling prior used for simulations a) with AFT data and b) with ZFT data.

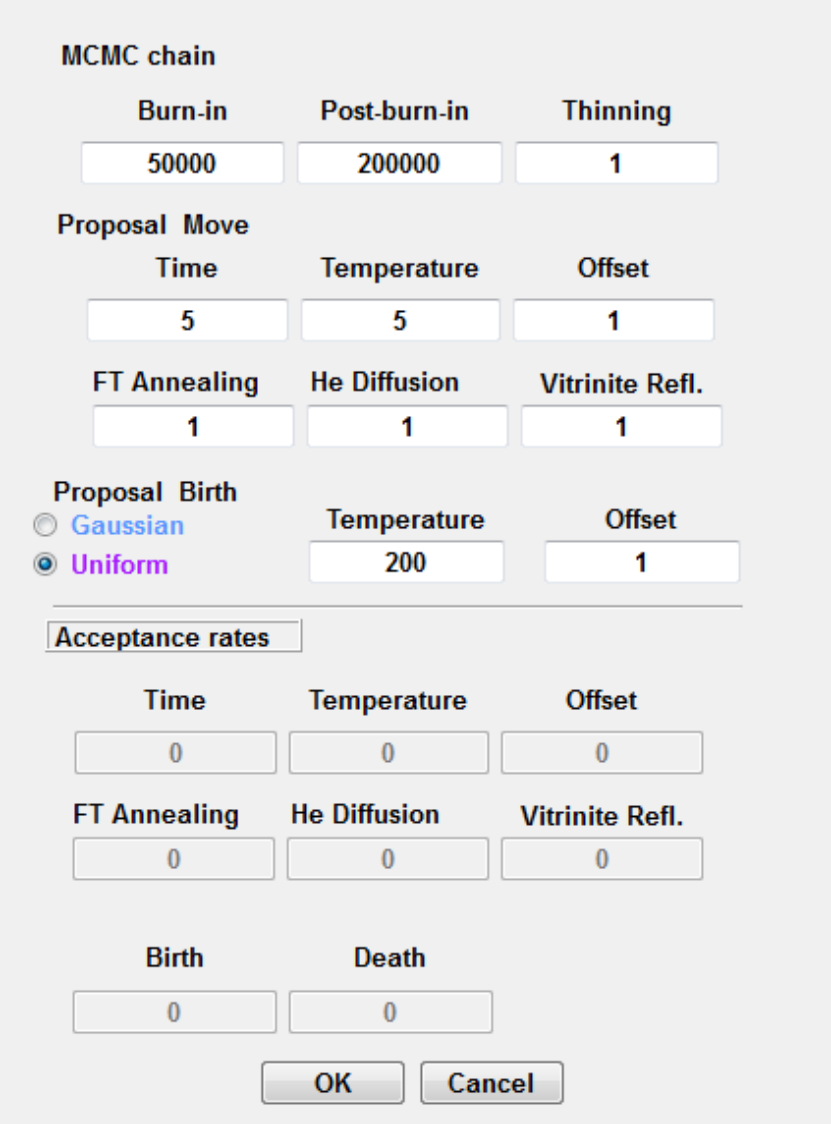

Fig. S2 - Markov chain Monte Carlo (MCMC) parameters used in the inverse modelling.

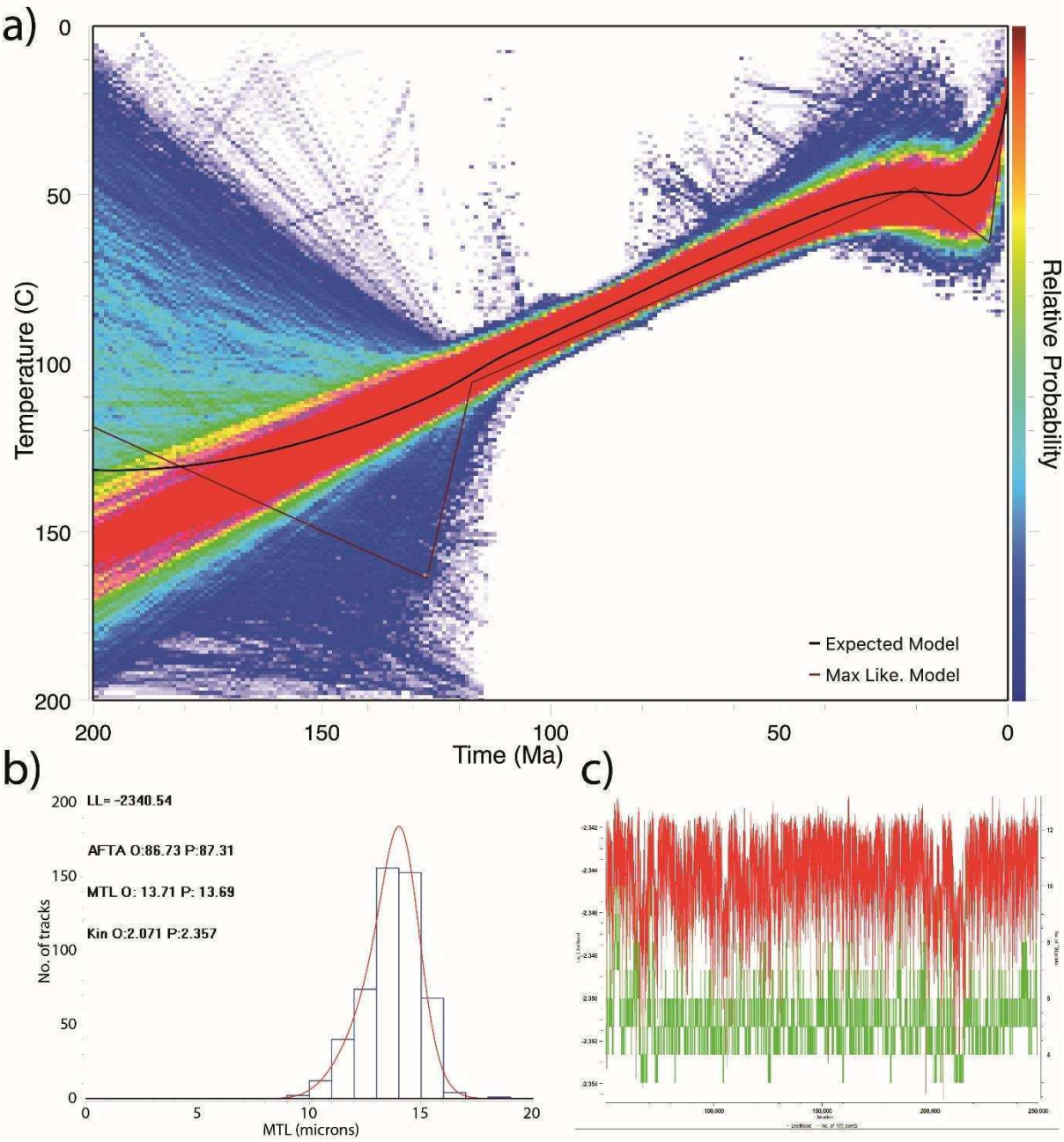

Fig. S3 – Scenario 1: thermal inverse modelling results constrained by AFT data from the AW group. a) Maximum Likelihood t-T path, expected t-T paths, and probability distribution of sampled thermal histories. b) Observed and predicted track length distribution, AFT age (AFTA), apatite mean track length (MTL), and apatite Dpar (Kin) (LL: log likelihood; O: observed; P: predicted). c) Log of the likelihood function and the number of time-temperature (T(t)) points as a function of iteration.

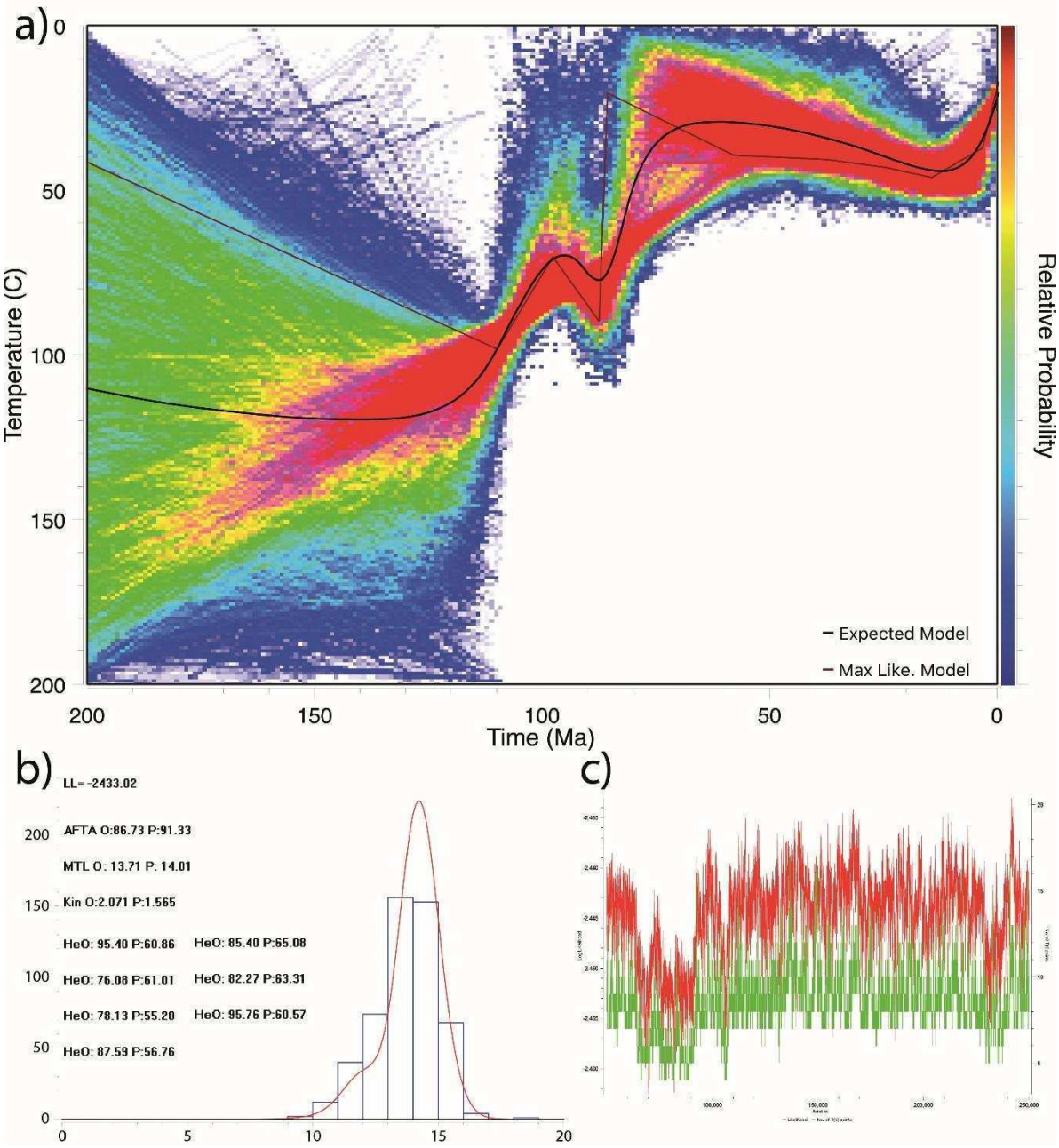

Fig. S4 – Scenario 2: thermal inverse modelling results constrained by AFT and AHe data from the AW group, without He kinetics. a) Maximum Likelihood t-T path, expected t-T paths, and probability distribution of sampled thermal histories. b) Observed and predicted track length distribution, AFT age (AFTA), apatite mean track length (MTL), apatite Dpar (Kin), and single grain AHe ages (LL: log likelihood; O: observed; P: predicted). c) Log of the likelihood function and the number of time-temperature (T(t)) points as a function of iteration.

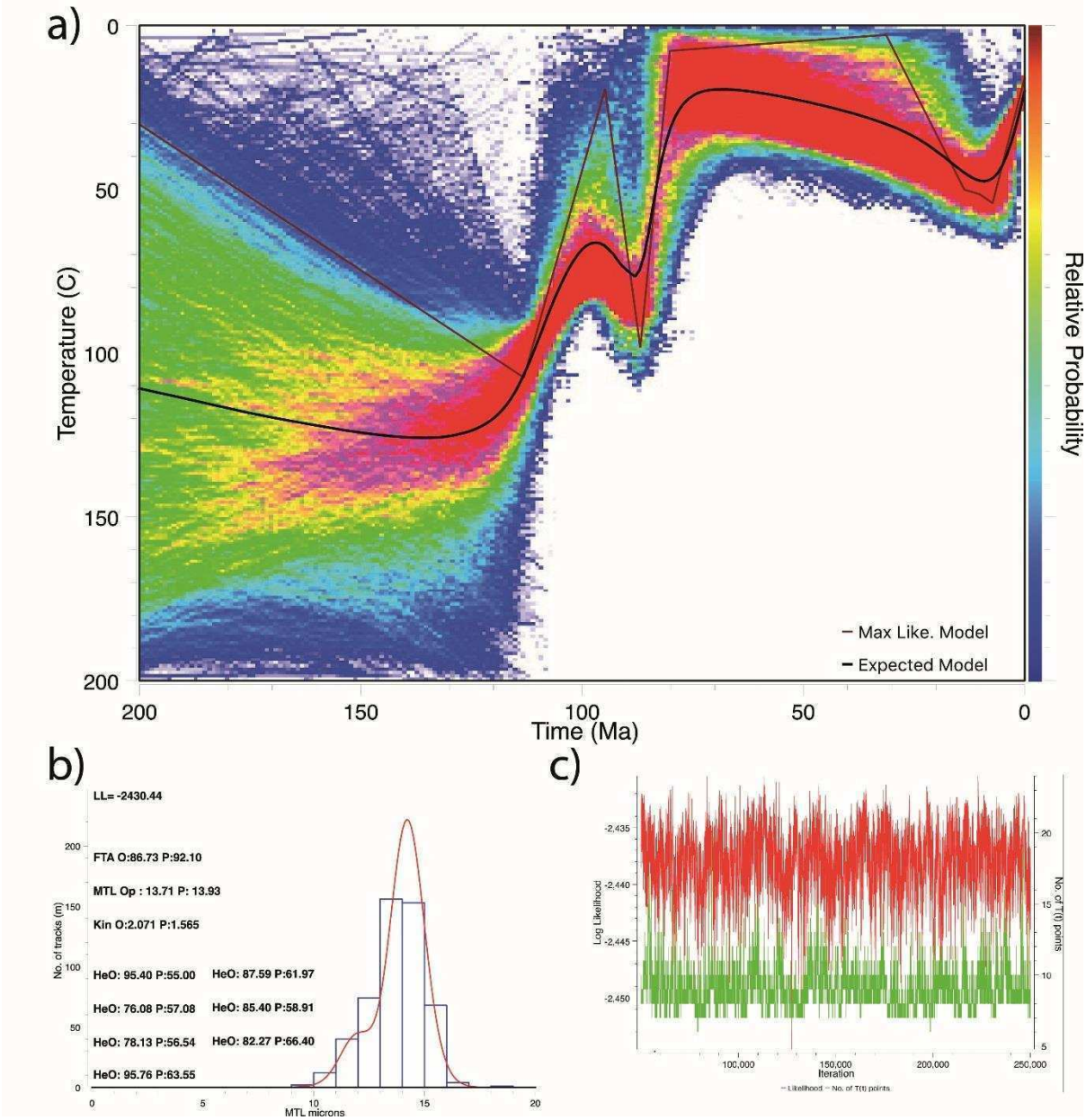

Fig. S5 – Scenario 3: thermal inverse modelling results constrained by AFT and AHe data from the AW group, using He kinetics of Gautheron et al. (2009). **a) Maximum Likelihood t-T path, expected t-T paths, and probability distribution of sampled thermal histories. b) Observed and predicted track length distribution, AFT age (AFTA), apatite mean track length (MTL), apatite Dpar (Kin), and single grain AHe ages (LL: log likelihood; O: observed; P: predicted). c) Log of the likelihood function and the number of time-temperature (T(t)) points as a function of iteration.**

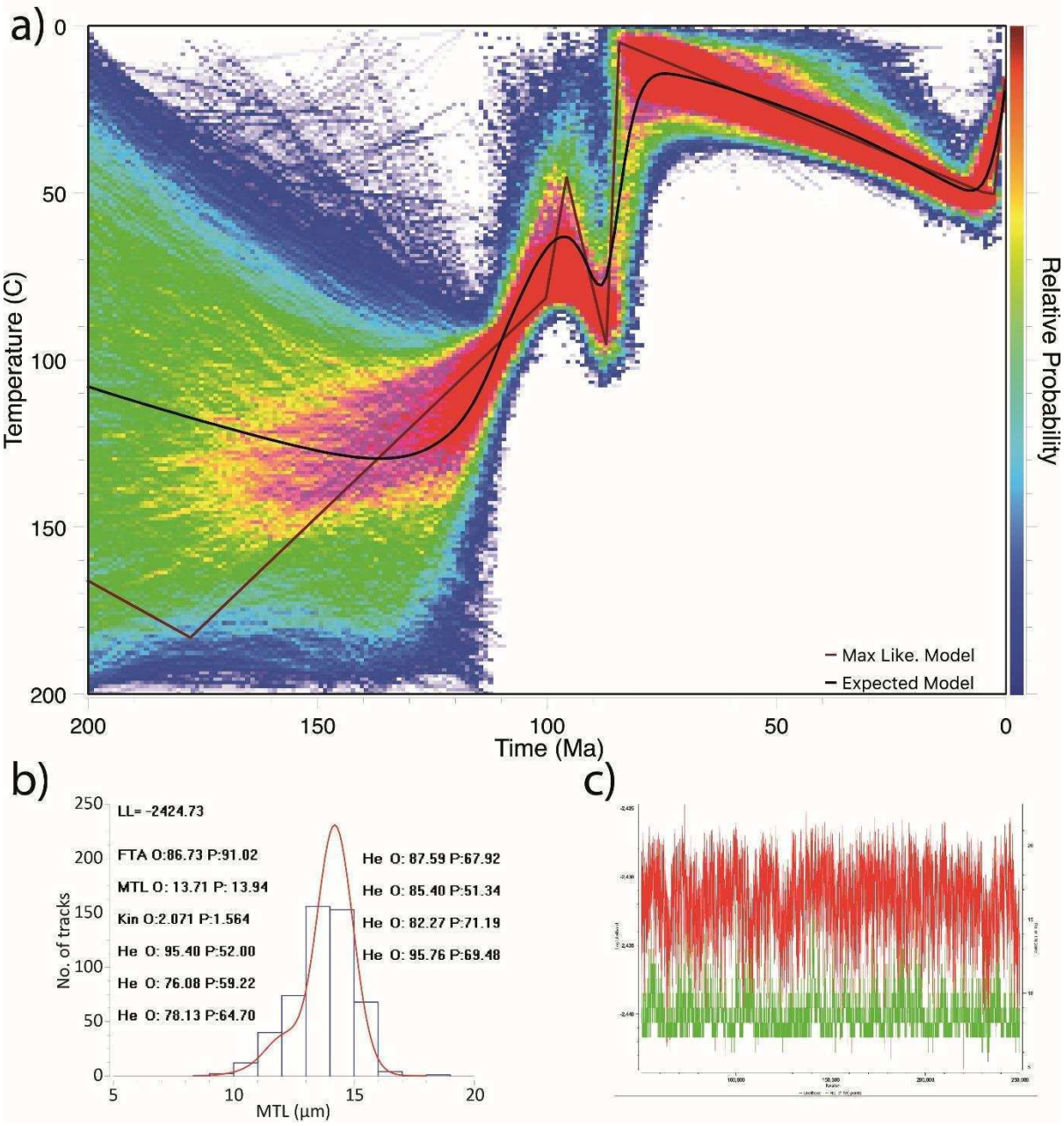

Fig. S6 – Scenario 4: thermal inverse modelling results constrained by AFT and AHe data from the AW group, using He kinetics of Flowers et al. (2009)**. a) Maximum Likelihood t-T path, expected t-T paths, and probability distribution of sampled thermal histories. b) Observed and predicted track length distribution, AFT age (AFTA), apatite mean track length (MTL), apatite Dpar (Kin), and single grain AHe ages (LL: log likelihood; O: observed; P: predicted). c) Log of the likelihood function and the number of time-temperature (T(t)) points as a function of iteration.**

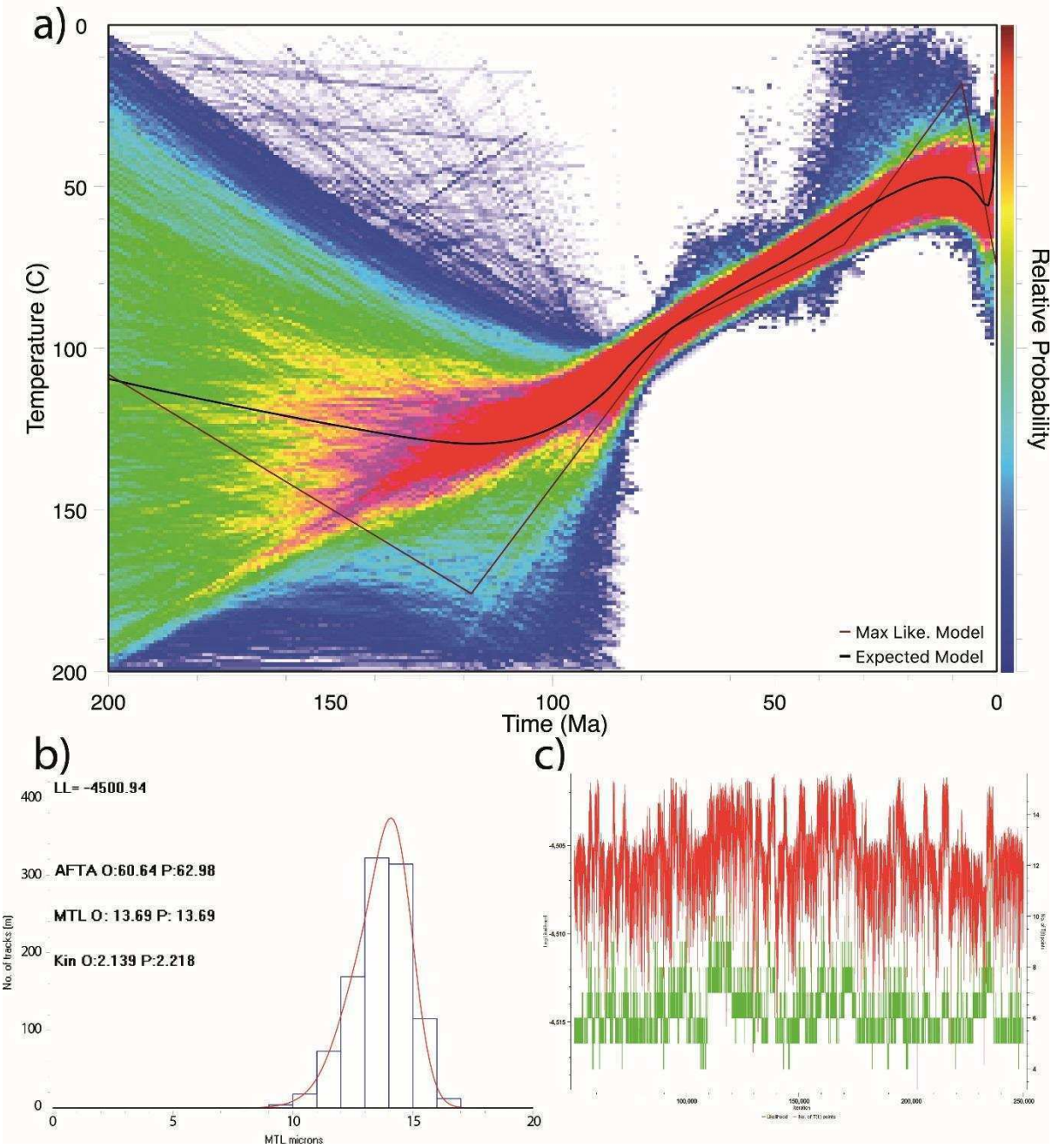

Fig. S7 – Scenario 5: thermal inverse modelling results constrained only by AFT data from the MS group. a) Maximum Likelihood t-T path, expected t-T paths, and probability distribution of sampled thermal histories. b) Observed and predicted track length distribution, AFT age (AFTA), apatite mean track length (MTL), and apatite Dpar (Kin) (LL: log likelihood; O: observed; P: predicted). c) Log of the likelihood function and the number of time-temperature (T(t)) points as a function of iteration.

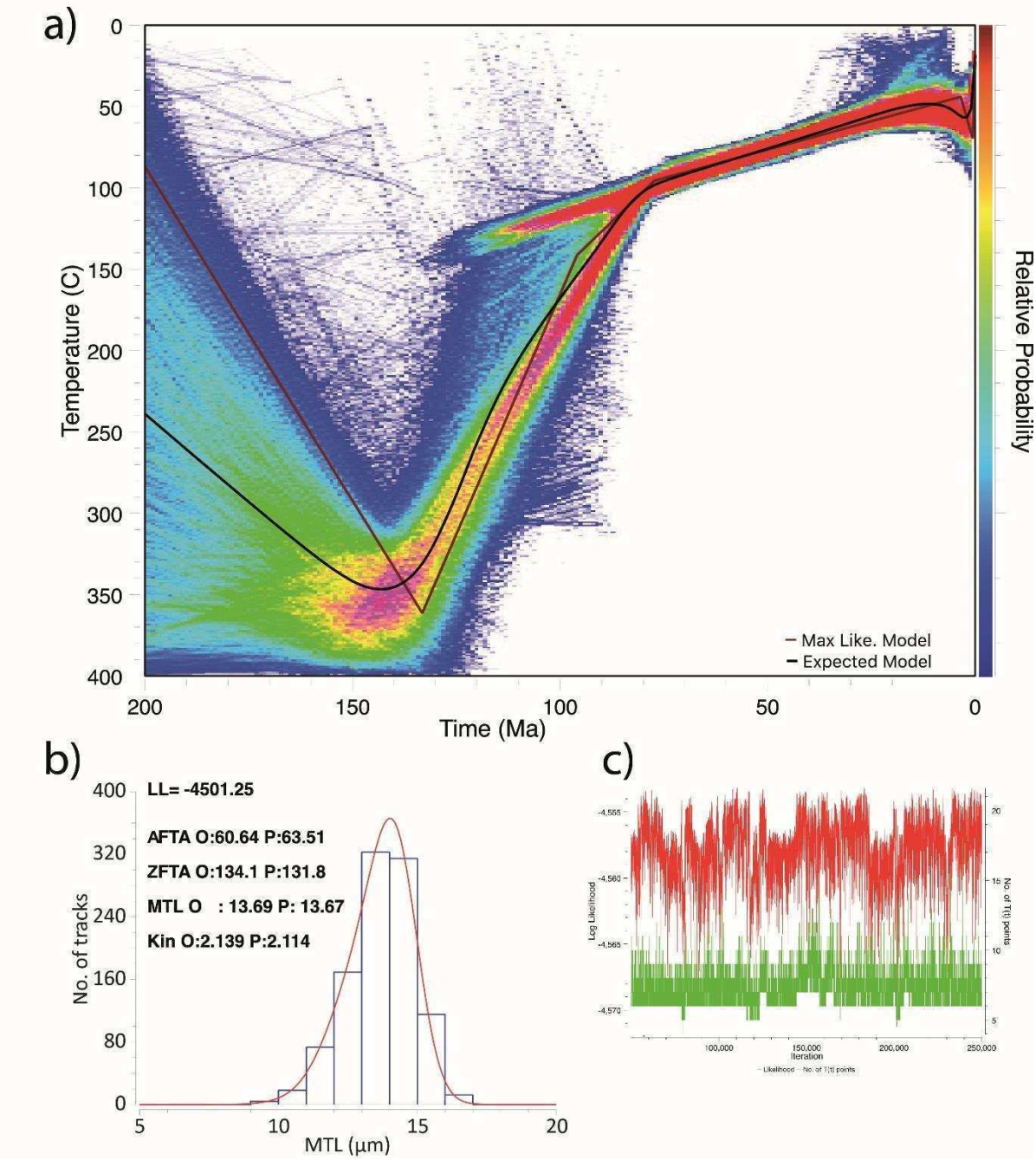

Fig. S8 – Scenario 6: thermal inverse modelling results constrained by AFT and ZFT data from the MS group, using ZFT annealing model of Yamada et al. (2007)**. a) Maximum Likelihood t-T path, expected t-T paths, and probability distribution of sampled thermal histories. b) Observed and predicted track length distribution, AFT age (AFTA), ZFT age (ZFTA), apatite mean track length (MTL), and apatite Dpar (Kin) (LL: log likelihood; O: observed; P: predicted). c) Log of the likelihood function and the number of time-temperature (T(t)) points as a function of iteration.**

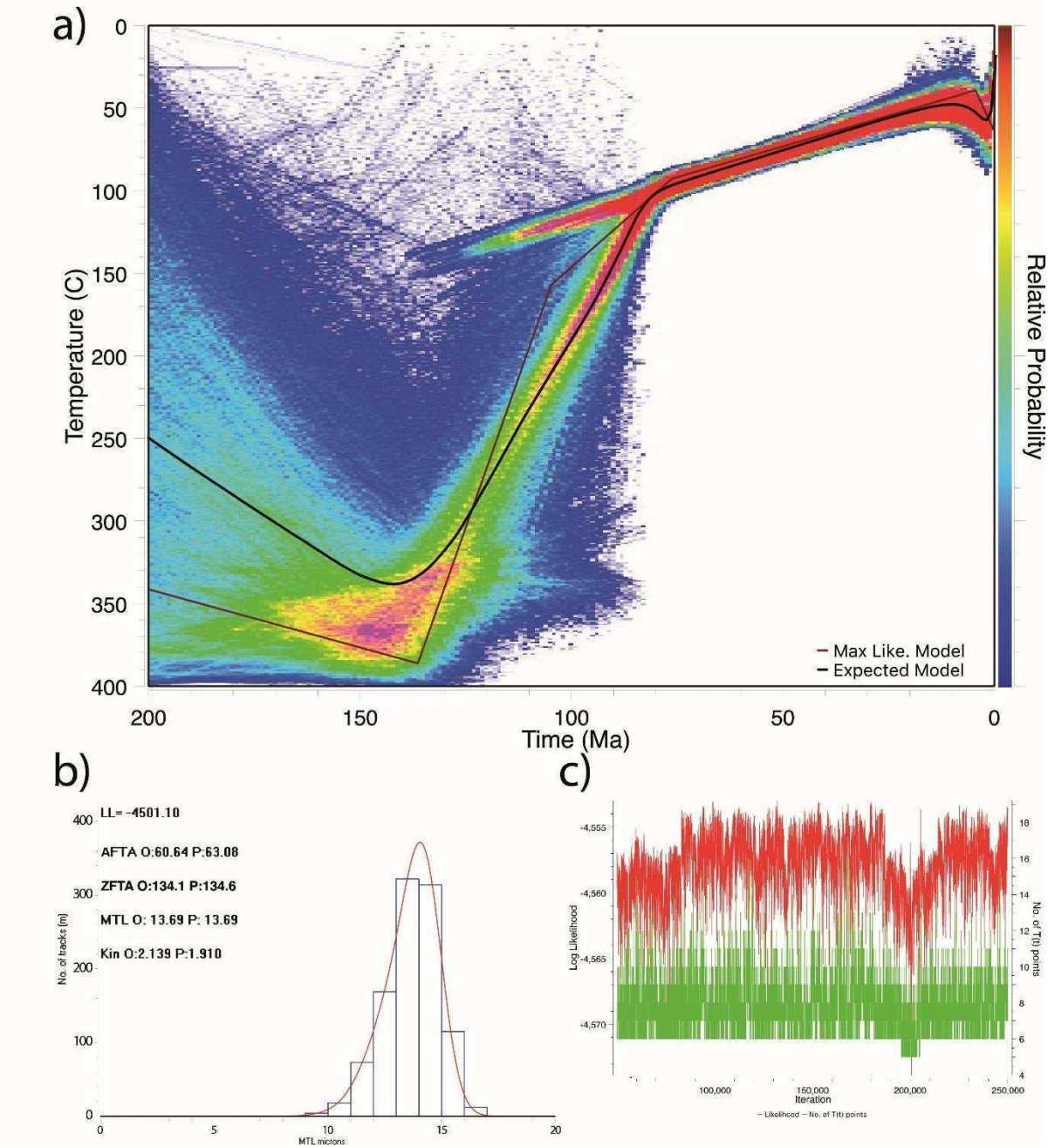

Fig. S9 – Scenario 6: thermal inverse modelling results constrained by AFT and ZFT data from the MS group, using ZFT annealing model of Tagami et al. (1988)**. a) Maximum Likelihood t-T path, expected t-T paths, and probability distribution of sampled thermal histories. b) Observed and predicted track length distribution, AFT age (AFTA), ZFT age (ZFTA), apatite mean track length (MTL), and apatite Dpar (Kin) (LL: log likelihood; O: observed; P: predicted). c) Log of the likelihood function and the number of time-temperature (T(t)) points as a function of iteration.**

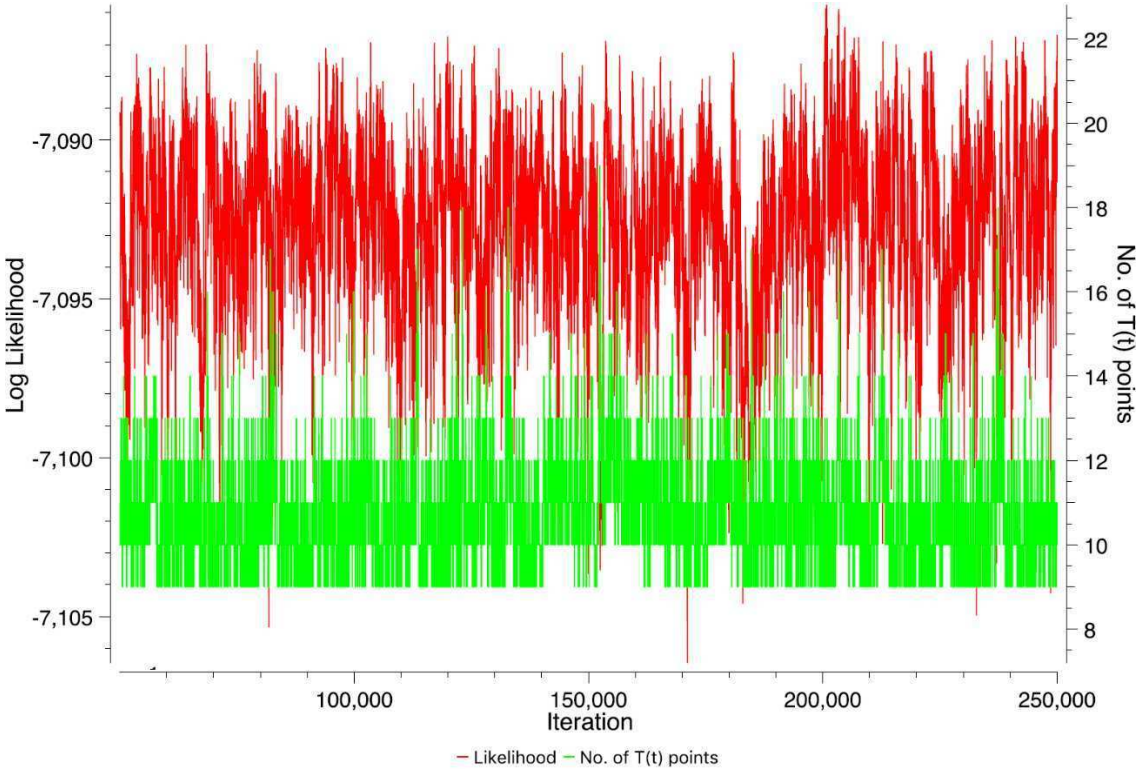

Fig. S10 - Log of the likelihood function and the number of time-temperature (T(t)) points as a function of iteration from the final model shown in Figure 5.